Table 3
Concentrations (ng/g lipid wt.) of OCs in Japanese human adipose tissues collected during 2003–04

	Male (n=18)			Female (n=10)		
	Mean±SD	Median	(Range)	Mean±SD	Median	(Range)
Age[a]	62±18	68	(25–81)	72±16	70	(53–109)
Lipid (%)	61±17	64	(11–82)	69±10	73	(50–81)
PCBs	1300±950	1100	(90–3100)	850±600	730	(380–2500)
p,p'-DDE	2500±2900	1500	(36–8900)	1300±1200	830	(110–3800)
p,p'-DDD	4.5±4.3	3.0	(<1.0–15)	1.3±1.5	0.65	(<1.0–4.1)
p,p'-DDT	56±65	39	(2.3–280)	19±15	15	(<1.0–48)
∑ DDTs	2600±2900	1500	(38–9000)	1300±1200	850	(120–3800)
α-HCH	1.8±2.2	1.5	(<1.0–9.2)	1.7±2.5	1.2	(<1.0–8.1)
β-HCH	870±920	620	(2.9–3800)	900±920	680	(110–3200)
∑ HCHs	870±920	630	(3.5–3800)	900±920	680	(110–3200)
oxychlordane	62±44	55	(3.6–150)	47±23	42	(18–86)
trans-nonachlor	220±160	230	(18–490)	150±130	110	(54–380)
cis-nonachlor	38±29	36	(3.0–89)	21±14	15	(7.7–49)
∑ CHLs	320±230	320	(23–730)	220±130	170	(80–510)
HCB	36±25	34	(1.6–84)	35±26	28	(12–100)

SD=standard deviation.
The concentrations below detection limit were treated as zero for arithmetic mean and median values. Concentrations of γ-HCH, *trans*- and *cis*-chlordane in all the samples were below detection limit.
[a] Year.

people are now being exposed to octa–deca-BDE congeners derived from these technical products.

3.2. Sex- and age-dependent accumulation

When concentrations of organohalogens in adipose tissues were compared between males and females, no sex difference was observed for OCs (Table 3). Even in the case of comparison using data from groups of similar age range (male: 49–81 years old, female: 53–83 years old), there was no statistically significant difference, although a weak significance (p=0.07) was shown for DDTs. This result was consistent with our previous report (Minh et al., 2001). This could be due to the fact that recent human exposure to OCs is relatively low and these contaminants in human tissues are in steady-state. In contrast, PBDE levels in males were significantly higher than those in females (Table 2). When groups of similar age range were compared, significantly higher concentrations of BDE209 were also observed in males. This implies that recent human exposure to PBDEs may be greater and these contaminants in human tissues do not attain steady-state. Hence, it is possible that breast-feeding might affect PBDE levels in adipose tissues of females. In an investigation on PBDEs in Japanese human milk, however, no significant difference in PBDE levels was observed between primiparas and multiparas (Eslami et al., 2006), indicating that PBDE elimination via breast-feeding may be relatively low. As other reasons why sex difference was observed for PBDEs, greater food intake and/or occupational exposure of males may be included. Unfortunately, we could not obtain information on the food habits and occupational histories of donors.

Generally, it is known that concentrations of OCs in human adipose tissues increase with age (Minh et al., 2001). Also in this study, age-dependent accumulation of OCs except CHLs were observed, while the correlation coefficients of PCBs and DDTs were slightly weak (Fig. 1). Because the ban of CHL usage was over ten years later (1986) than those of other OCs and technical CHL was mainly used for timber houses as a termiticide, certain Japanese people might have been specifically exposed to CHLs. Actually, we demonstrated that pet dogs and cats, which are closely associated with human environment, and raccoon dogs, which inhabit the vicinity of human houses, accumulated relatively higher levels of CHLs compared with other OCs, indicating that pollution sources of CHLs are still present in and/or near CHL treated houses (Kunisue et al., 2005, 2007).

No age-dependent accumulation of total PBDEs (Fig. 1) or each BDE congener (data not shown) was found either. As described above, significant sex differences in the accumulation levels of PBDEs were shown and hence we examined the data on males and females individually, but no age-dependent accumulation of PBDEs was found in both sexes. Eslami et al. (2006) also reported that PBDE levels in Japanese human milk did not increase with age. In Japan, technical tetra- and octa-BDE products were used as flame retardants until 1990 and 1999, respectively, and technical deca-BDE is in use even now (Watanabe and Sakai, 2003). In addition, PBDEs were detected in various Japanese environmental media (Watanabe and Sakai, 2003). Considering these observations, recent human exposure to PBDEs may be the most possible reason why no age-dependent accumulation of PBDEs was shown in this study. The fact that no age-dependent accumulation of PBDEs was observed in human adipose tissues has been also reported in USA (Johnson-Restrepo et al., 2005; She et al., 2002), Belgium (Covaci et al., 2002; Naert et al., 2006), and Spain (Fernandez et al., 2007), and recent human exposure to these contaminants is stated as the reason in their studies also. As described later, specific accumulation kinetics by PBDE congeners in human bodies may be another possible reason.

3.3. Congener profile of PBDEs

PBDE compositions of human adipose tissues analyzed in this study are shown in Fig. 2. BDE-153 was the dominant isomer, followed by BDE-47 and BDE-209. To our knowledge, this is the first study that octa–deca-BDE congeners were detected in Japanese adipose tissues. Interestingly, BDE-197 and 207 were also detected with relatively high levels (Fig. 2). Considering that these isomers are present abundantly in technical octaBDE (La Guardia et al., 2006), it is likely that the relatively high composition of BDE-197 and BDE-207 in adipose tissues reflected the exposure originating from this technical product.

It has been reported that relatively higher proportion of BDE-153 was also observed in human adipose tissues from Belgium (Covaci et al., 2002; Naert et al., 2006), Spain (Fernandez et al., 2007), and

Table 4
International comparison of PBDE levels (ng/g lipid wt.) in human adipose tissue

Country	Collected Year	Sex[a]	Age (Year)	*n*	Lipid (%)	BDE15	BDE28	BDE47	BDE99	BDE100	BDE153	BDE154	BDE183	BDE196	BDE197	BDE206	BDE207	BDE209	BDE-47+99+153	Ref.
Japan	2003–2004	M, F	25–109	28	66	0.12	0.17	0.79	0.13	0.29	1.2	0.11	0.10	0.075	0.41	0.052	0.36	0.92	2.1	This study
Japan	2000	F	40–60	10	72–95	NA	0.076	0.46	0.12	0.25	0.38	0.060	0.047	NA	NA	NA	NA	NA	0.96	Choi et al. (2003)
Belgium	2001–2003	M, F	19–84	53	NA	NA	0.20	0.88	0.47	0.72	2.4	0.93	0.78	NA	NA	NA	NA	NA	3.8	Naert et al. (2006)
Belgium	2000	M, F	19–77	20	94	NA	<0.05	1.1	0.18	0.35	2.3	<0.30	NA	NA	NA	NA	NA	NA	3.6	Covaci et al. (2002)
USA (New York)	2003–2004	M, F	18–51	52	58	NA	1.9	29	10	12	<1.0	<1.0	NA	NA	NA	NA	NA	ND	39	Johnson-Restrepo et al. (2005)
USA (San Francisco)	1996–1998	F	28–62	23	72	NA	NA	18	6.6	3.2	4.1	6.4	NA	NA	NA	NA	NA	NA	29	She et al. (2002)
Singapore	2003–2004	F	22–41	16	81	NA	NA	2.0	ND	<0.70	ND	ND	NA	NA	NA	NA	NA	NA	2.0	Li et al. (2005)
Sweden	1994	M, F	47–83	5	56–84	NA	0.080	2.3	1.4	0.25	1.1	0.060	NA	NA	NA	NA	NA	NA	4.8	Guvenius et al. (2001)
Finland	NA	M, F	14–95	37	NA	NA	NA	0.55	0.74	NA	0.30	NA	NA	NA	NA	NA	NA	NA	1.6	Smeds and Saukko (2003)
Spain	2003	F	24–81	20	79	NA	0.046	0.63	0.24	0.20	1.3	0.034	0.35	NA	NA	NA	NA	NA	2.2	Fernandez et al. (2007)

NA; no data available. ND; not detected.
[a] M; Male, F; Female.

Sweden (Guvenius et al., 2001). But, in the United States, where greater amounts of technical pentaBDE have been used, BDE-47 accumulation was prominent in human adipose tissues (Johnson-Restrepo et al., 2005; She et al., 2002). Thus, it seems that PBDE profiles in human adipose tissues at least partly reflect the usage of technical PBDE products in the past. However, in technical octaBDE, which is considered as the main pollution source of BDE-153, BDE-183 and BDE-197 are present more abundantly than BDE-153 (La Guardia et al., 2006). In addition, it was reported that higher levels of BDE-47 than BDE-153 were detected in Japanese human milk and BDE-209 was the dominant isomer in Japanese human blood (Inoue et al., 2006); these PBDE patterns were different from those observed in the adipose tissues of this study (Fig. 2). Considering that PBDE profiles in human blood reflect the recent exposure (Petreas et al., 2003; Takasuga et al., 2004), it is likely that human exposure to BDE-209 derived from technical deca-BDE, which is in use even now, is more pronounced in Japan. Therefore, biotransformation and accumulation kinetic properties of each PBDE congeners after human exposure to PBDEs also contribute to PBDE patterns in human tissues. Inoue et al. (2006) showed using Quantitative Structure Activity Relationship (QSAR) analysis, that the PBDE and PCB transfer rates from human blood to milk could become lower with increasing number of hydrogen-bond acceptor and octanol/water partition coefficient (Kow), indicating lower transfer of higher brominated congeners such as BDE-209 from blood to milk. In addition, it was reported that the half-life of BDE-209 in human blood was shorter compared with other PBDE congeners (Thuresson et al., 2006), and it was indicated that debromination of BDE-209 may occur in human bodies (Thuresson et al., 2005). Actually, in studies using Sprague–Dawley rats, the rapid biotransformation of BDE-209 such as debromination to octa–nona-BDEs and formation of hydroxyl and guaiacol metabolites was observed (Mörck et al., 2003; Sandholm et al., 2003). Furthermore, Mörck et al. (2003) reported that higher concentrations of BDE-209 were found in blood and blood-rich organs such as liver and the adipose

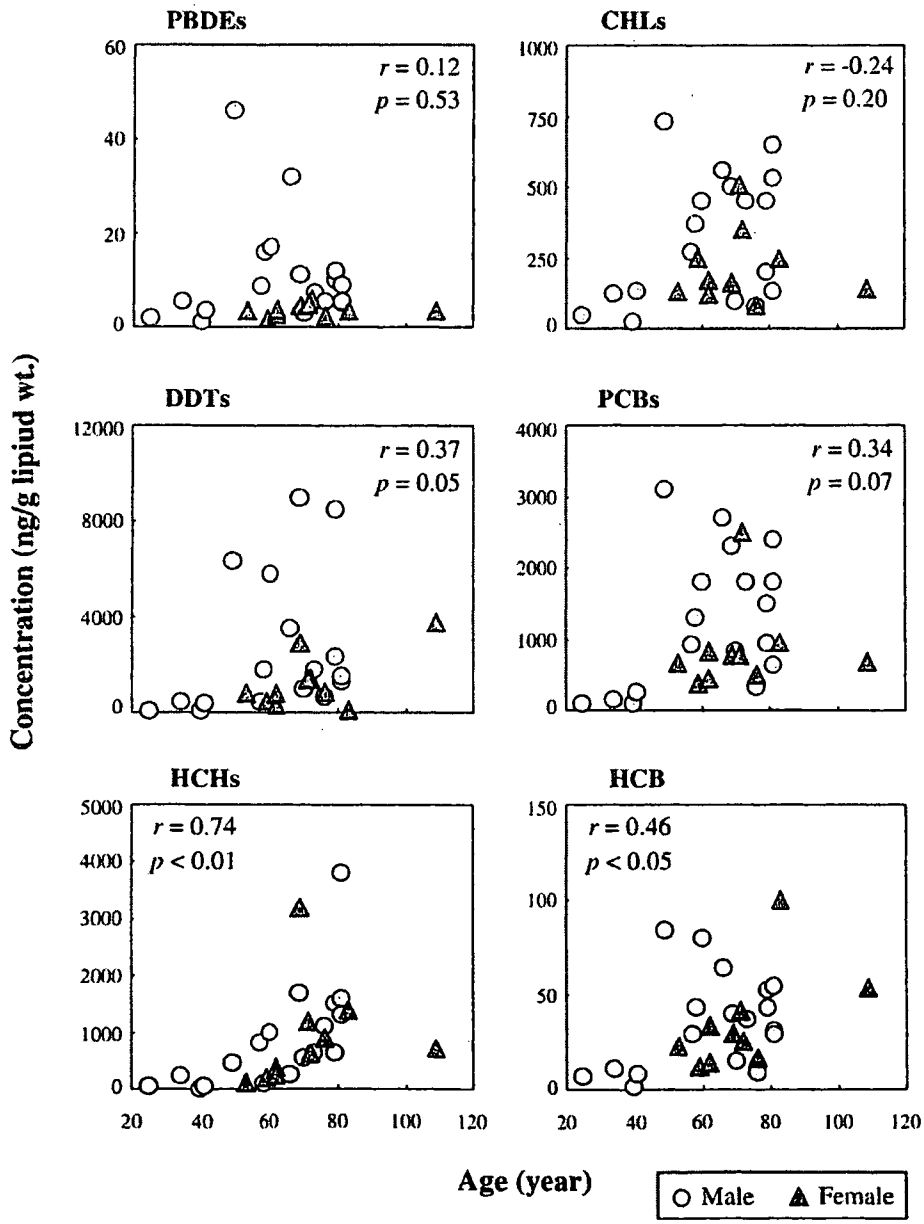

Fig. 1. Relationships between age and concentrations of organohalogen compounds in Japanese human adipose tissues.

tissue had the lowest concentrations in these experimental rats. From these observations, it can be anticipated that the distribution of BDE-209 to adipose tissues may be relatively low in humans also because of the rapid biotransformation and/or binding to proteins, although BDE-209 is pronounced in human blood after the intake of this compound. In contrast, it was estimated that the half-life of BDE-153 in rat and human adipose tissues was the longest among other tetra–hexa-BDE congeners (Geyer et al., 2004), and hence it is likely that BDE-153 is more persistent and lipid-dependently accumulated in human bodies. The difference in PBDE patterns among human blood, milk, and tissues was also reported in Sweden (Guvenius et al., 2001).

Variations in PBDE compositions were found in adipose tissues analyzed in this study (Fig. 2). This could be due to the different exposure profiles of PBDEs by individuals in the past, as a main cause. However, considering that donors died of disease, it is possible that the effects by disease, *e.g.* defective hepatic metabolism, may affect tissue distribution of PBDEs, especially BDE209 because of rapid biotransformation. Therefore, detailed studies on tissue distribution of PBDE congeners in individual subjects are needed to elucidate the kinetic properties of these contaminants in human bodies. Furthermore, considering recent human exposure to BDE-209 in Japan (Takasuga et al., 2004), the rapid biotransformation to hydroxylated PBDEs (OH-PBDEs) (Mörck et al., 2003; Sandholm et al., 2003), and higher contribution to thyroid hormone homeostasis disturbance of OH-PBDEs rather than PBDEs (Legler and Brouwer, 2003), the investigations on PBDE metabolites in Japanese citizens may be also indispensable in the future.

3.4. Relationship between PBDEs and organochlorines

In studies on human adipose tissues of Belgium and the United States, no significant relationship was observed between PBDEs and PCBs, indicating human exposure to PBDEs via not only diet but also inhalation of indoor air and dust (Naert et al., 2006; Johnson-Restrepo et al., 2005). Recently, some studies on PBDEs in indoor air (Butt et al., 2004; Wilford et al., 2004) and dust (Schecter et al., 2005; Stapleton et al., 2005) have been conducted and it has been pointed out that the inhalation of indoor air and dust could be a potential human exposure route to PBDEs. In fact, significantly higher levels of PBDEs were detected in blood of workers, who work in the factory using technical PBDE, than the general public (Thuresson et al., 2005, 2006).

When the relationships between PBDEs and OCs in Japanese adipose tissues analyzed in this study were examined, significant correlations were found between PBDEs and PCBs and other OCs except HCHs (Table 5). These results were different from the observations reported in the United States (Johnson-Restrepo et al., 2005) and Belgium (Naert et al., 2006). This indicates that human exposure routes to PBDEs and OCs are almost similar in Japan. As for the weak correlations between HCHs and other organohalogens, it is speculated that HCHs, which are relatively lower lipophilic OCs (Kow 3.8–4.1; Kelly and Gobas, 2001), are easily expelled from adipose tissues compared with other OCs (Kow 5.5–8.1; Kelly and Gobas, 2001) and PBDEs (Kow 5.8–9.9; Inoue et al., 2006). It has been reported that the major exposure sources for Japanese to OCs such as dioxins and PCBs were via fish intake (Tsutsumi et al., 2001) and concentrations of these contaminants in Japanese human milk increased with the frequency of fish intake (Takekuma et al., 2004). Likewise, Ohta et al. (2002) reported that concentrations of PBDEs in fishes were higher than those in other food items from Japan and fish intake-dependent increase of PBDE levels in human milk were shown, suggesting that fish intake significantly contributes to human exposure to PBDEs in Japan. Because Japanese donors in this study might be also exposed to PBDEs and OCs possibly via fish intake, it seems that significant correlations among these organohalogen contaminants were

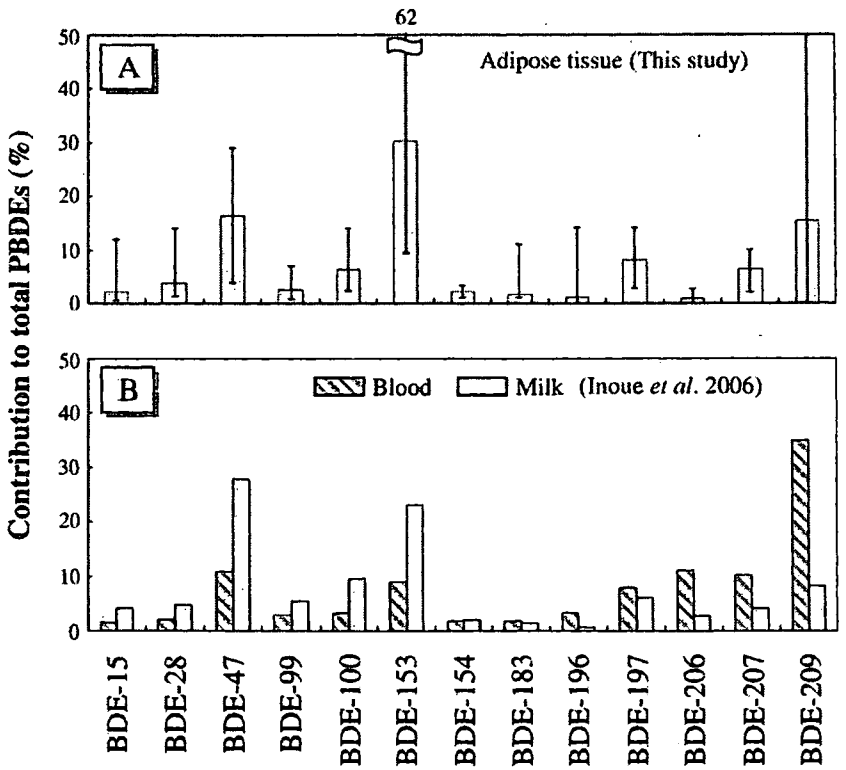

Fig. 2. Compositions of PBDEs in human adipose tissues analyzed in this study (A) and those in Japanese human milk and blood reported previously (B). Error bars show ranges.

Table 5
Spearman's rank correlation (r value) between PBDEs and OCs in Japanese human adipose tissues

	DDTs	PCBs	HCHs	CHLs	HCB
PBDEs	0.732***	0.726***	0.314	0.705***	0.635**
DDTs	–	0.68***	0.442*	0.625**	0.709***
PCBs	–	–	0.384*	0.871****	0.76****
HCHs	–	–	–	0.337	0.433*
CHLs	–	–	–	–	0.747***

* $p<0.05$.
** $p<0.01$.
*** $p<0.001$.
**** $p<0.0001$.

found in adipose tissues. However, Ohta et al. (2002) did not analyze hepta–deca-BDE congeners in Japanese food items and human milk. In addition, it was reported more recently that PBDEs were detected with high levels in Japanese house and office dusts (Suzuki et al., 2006). Therefore, comprehensive investigations on human exposure routes to PBDEs are needed in Japan.

4. Conclusion

We elucidated contamination status and accumulation features of PBDEs and OCs in Japanese human adipose tissues collected during 2003–04. PBDE levels observed in this study were relatively higher than in specimens collected during 2000, indicating recent human exposure to PBDEs in Japan. In addition, accumulation of octa–deca-BDE congeners was found in Japanese human adipose tissues for the first time. BDE-153 was the dominant isomer in adipose tissues, but this trend was different from those in human milk (BDE-47) and blood (BDE-209) reported previously in Japan, implying the congener-specific kinetics in human bodies. Investigations on toxicokinetics including the distribution to various organs and tissues in addition to continuous monitoring and exposure source surveys of PBDEs in humans are essential to assess the organ-specific toxicological risks of PBDE congeners.

Acknowledgements

We express our heartfelt gratitude to the families of the donors. We also thank the doctors and medical officers in Ehime University Graduate School of Medicine and School of Medicine, Keio University for their help in sample collection. The authors are thankful to Dr. An. Subramanian (CMES, Ehime University) for critical reading of this manuscript. This study was supported by the Global Environmental Research Fund (RF-064) and the Waste Management Research Grant (K1821 and K1836) from the Ministry of the Environment and by Grants-in-Aid for Scientific Research (A) (No.16201014) and (B) (No. 18310046), Young Scientists (B) (Project 19780239) and "Global COE Program" from the Ministry of Education, Culture, Sports, Science and Technology, and Japan Society for the Promotion of Science (JSPS), and by Grants-in-Aid for Scientific Research (H14-013) from the Ministry of Health, Labour and Welfare, Japan.

References

Akutsu K, Kitagawa M, Nakazawa H, Makino T, Iwazaki K, Oda H, et al. Time-trend (1973–2000) of polybrominated diphenyl ethers in Japanese mother's milk. Chemosphere 2003;53:645–54.

Butt CM, Diamond ML, Truong J, Ikonomou MG, Ter Schure AFH. Spatial distribution of polybrominated diphenyl ethers in Southern Ontario as measured in indoor and outdoor window organic films. Environ Sci Technol 2004;38:724–31.

Choi J, Fujimaki S, Kitamura K, Hashimoto S, Ito H, Suzuki N, et al. Polybrominated dibenzo-*p*-dioxins, dibenzofurans, and diphenyl ethers in Japanese human adipose tissue. Environ Sci Technol 2003;37:817–21.

Covaci A, de Boer J, Ryan JJ, Voorspoels S, Schepens P. Distribution of organobrominated and organochlorinated contaminants in Belgian human adipose tissue. Environ Res 2002;88:210–8.

Darnerud PO. Toxic effects of brominated flame retardants in man and wildlife. Environ Int 2003;29:841–53.

Eslami B, Koizumi A, Ohta S, Inoue K, Aozasa O, Harada K, et al. Large-scale evaluation of the current level of polybrominated diphenyl ethers (PBDEs) in breast milk from 13 regions of Japan. Chemosphere 2006;63: 554–61.

Fernandez MF, Araque P, Kiviranta H, Molina-Molina JM, Rantakokko P, Laine O, et al. PBDEs and PBBs in the adipose tissue of women from Spain. Chemosphere 2007;66:377–83.

Geyer HJ, Schramm K-W, Darnerud PO, Aune M, Feicht EA, Fried KW, et al. Terminal elimination half-lives of the brominated flame retardants TBBPA, HBCD, and lower brominated PBDEs in humans. Organohalog Compd 2004;66:3820–5.

Gill U, Chu I, Ryan JJ, Feeley M. Polybrominated diphenyl ethers: human tissue levels and toxicology. Rev Environ Contam Toxicol 2004;183:55–97.

Guvenius DM, Bergman Å, Norén K. Polybrominated diphenyl ethers in Swedish human liver and adipose tissue. Arch Environ Contam Toxicol 2001;40:564–70.

Inoue K, Harada K, Takenaka K, Uehara S, Kono M, Shimizu T, et al. Levels and concentration ratios of polychlorinated biphenyls and polybrominated diphenyl ethers in serum and breast milk in Japanese mothers. Environ Health Perspect 2006;114:1179–85.

Johnson-Restrepo B, Kannan K, Rapaport DP, Rodan BD. Polybrominated diphenyl ethers and polychlorinated biphenyls in human adipose tissue from New York. Environ Sci Technol 2005;39:5177–82.

Kelly BC, Gobas FAPC. Bioaccumulation of persistent organic pollutants in lichen–caribou–wolf food chains of Canada's central and western Arctic. Environ Sci Technol 2001;35:325–34.

Kunisue T, Nakanishi S, Watanabe M, Abe T, Nakatsu S, Kawauchi S, et al. Contamination status and accumulation features of persistent organochlorines in pet dogs and cats from Japan. Environ Pollut 2005;136: 465–76.

Kunisue T, Takayanagi N, Tsubota T, Tanabe S. Persistent organochlorines in raccoon dogs (*Nyctereutes procyonoides*) from Japan: hepatic sequestration of oxychlordane. Chemosphere 2007;66:203–11.

La Guardia MJ, Hale RC, Harvey E. Detailed polybrominated diphenyl ether (PBDE) congener composition of the widely used penta-, octa-, and deca-BDE technical flame-retardant mixtures. Environ Sci Technol 2006;40: 6247–54.

Law RJ, Alaee M, Allchin CR, Boon JP, Lebeuf M, Lepom P, et al. Levels and trends of polybrominated diphenylethers and other brominated flame retardants in wildlife. Environ Int 2003;29:757–70.

Legler J, Brouwer A. Are brominated flame retardants endocrine disruptors? Environ Int 2003;29:879–85.

Li QQ, Loganath A, Chong YS, Obbard JP. Determination and occurrence of polybrominated diphenyl ethers in maternal adipose tissue from inhabitants of Singapore. J Chromatogr B 2005;819:253–7.

Minh TB, Watanabe M, Tanabe S, Yamada T, Hata J, Watanabe S. Specific accumulation and elimination kinetics of *tris*(4-chlorophenyl)methane, *tris* (4-chlorophenyl)methanol and other persistent organochlorines in humans from Japan. Environ Health Perspect 2001;109:927–35.

Mörck A, Hakk H, Örn U, Klasson Wehler E. Decabromodiphenyl ether in the rat: absorption, distribution, metabolism, and excretion. Drug Metab Dispos 2003;31:900–7.

Naert C, Piette M, Bruneel N, Van Peteghem C. Occurrence of polychlorinated biphenyls and polybrominated diphenyl ethers in Belgian human adipose tissue samples. Arch Environ Contam Toxicol 2006;50:290–6.

Ohta S, Ishizuka D, Nishimura H, Nakao T, Aozasa O, Shimidzu Y, et al. Comparison of polybrominated diphenyl ethers in fish, vegetables, and meats and levels in human milk of nursing women in Japan. Chemosphere 2002;46:689–96.

Petreas M, She J, Brown FR, Winkler J, Windham G, Rogers E, et al. High body burdens of 2,2′,4,4′-tetrabromodiphenyl ether (BDE-47) in California women. Environ Health Perspect 2003;111:1175–9.

Sandholm A, Emanuelsson B-M, Klasson Wehler E. Bioavailability and half-life of decabromodiphenyl ether (BDE-209) in rat. Xenobiotica 2003;33:1149–58.

Schecter A, Päpke O, Joseph JE, Tung K-C. Polybrominated diphenyl ethers (PBDEs) in U.S. computers and domestic carpet vacuuming: possible sources of human exposure. J Toxicol Environ Health Part A 2005;68:501–13.

She J, Petreas M, Winkler J, Visita P, McKinney M, Kopec D. PBDEs in the San Francisco Bay area: measurements in harbor seal and human breast adipose tissue. Chemosphere 2002;46:697–707.

Smeds A, Saukko P. Brominated flame retardants and phenolic endocrine disrupters in Finnish human adipose tissue. Chemosphere 2003;53: 1123–30.

Sjödin A, Patterson Jr DG, Bergman Å. A review on human exposure to brominated flame retardants-particularly polybrominated diphenyl ethers. Environ Int 2003;29:829–39.

Stapleton HM, Dodder NG, Offenberg JH, Schantz MM, Wise SA. Polybrominated diphenyl ethers in house dust and clothes dryer lint. Environ Sci Technol 2005;39:925–31.

Suzuki G, Nose K, Takigami H, Takahashi S, Sakai S-I. PBDEs and PBDD/Fs in house and office dust from Japan. Organohalog Compd 2006;68:1843–6.

Takasuga T, Senthilkumar K, Takemori H, Ohi E, Tsuji H, Nagayama J. Impact of fermented brown rice with *Aspergillus oryzae* (FEBRA) intake and concentrations of polybrominated diphenylethers (PBDEs) in blood of humans from Japan. Chemosphere 2004;57:795–811.

Takekuma M, Saito K, Ogawa M, Matsumoto R, Kobayashi S. Levels of PCDDs, PCDFs, and Co-PCBs in human milk in Saitama, Japan, and epidemiological research. Chemosphere 2004;54:127–35.

Tanabe S. Environmental Specimen Bank in Ehime University (es-Bank), Japan for global monitoring. J Environ Monit 2006;8:782–90.

Thuresson K, Bergman Å, Jakobsson K. Occupational exposure to commercial decabromodiphenyl ether in workers manufacturing or handling flame-retarded rubber. Environ Sci Technol 2005;39:1980–6.

Thuresson K, Höglund P, Hagmar L, Sjödin A, Bergman Å, Jakobsson K. Apparent half-lives of hepta- to decabrominated diphenyl ethers in human serum as determined in occupationally exposed workers. Environ Health Perspect 2006;114:176–81.

Tsutsumi T, Yanagi T, Nakamura M, Kono Y, Uchibe H, Iida T, et al. Update of daily intake of PCDDs, PCDFs, and dioxin-like PCBs from food in Japan. Chemosphere 2001;45:1129–37.

Ueno D, Kajiwara N, Tanaka H, Subramanian A, Fillmann G, Lam PKS, et al. Global pollution monitoring of polybrominated diphenyl ethers using skipjack tuna as a bioindicator. Environ Sci Technol 2004;38:2312–6.

Watanabe I, Sakai S. Environmental release and behavior of brominated flame retardants. Environ Int 2003;29:665–82.

Wilford BH, Harner T, Zhu J, Shoeib M, Jones KC. Passive sampling survey of polybrominated diphenyl ether flame retardants in indoor and outdoor air in Ottawa, Canada: implications for sources and exposure. Environ Sci Technol 2004;38:5312–8.

Humanized Anti-CD26 Monoclonal Antibody as a Treatment for Malignant Mesothelioma Tumors

Teruo Inamoto,[1,3] Taketo Yamada,[2] Kei Ohnuma,[1] Shinichiro Kina,[1] Nozomu Takahashi,[1] Tadanori Yamochi,[1] Sakiko Inamoto,[1,3] Yoji Katsuoka,[3] Osamu Hosono,[1] Hirotoshi Tanaka,[1] Nam H. Dang,[4] and Chikao Morimoto[1,4]

Abstract **Purpose:** CD26 is a 110-kDa cell surface antigen with a role in tumor development. In this report, we show that CD26 is highly expressed on the cell surface of malignant mesothelioma and that a newly developed humanized anti-CD26 monoclonal antibody (mAb) has an inhibitory effect on malignant mesothelioma cells in both *in vitro* and *in vivo* experiments.

Experimental Design: Using immunohistochemistry, 12 patients' surgical specimens consisting of seven malignant mesothelioma, three reactive mesothelial cells, and two adenomatoid tumors were evaluated for expression of CD26. The effects of CD26 on malignant mesothelioma cells were assessed in the presence of transfection of CD26-expressing plasmid, humanized anti-CD26 mAb, or small interfering RNA against CD26. The *in vivo* growth inhibitory effect of humanized anti-CD26 mAb was assessed in human malignant mesothelioma cell mouse xenograft models.

Results: In surgical specimens, CD26 is highly expressed in malignant mesothelioma but not in benign mesothelial tissues. Depletion of CD26 by small interfering RNA results in the loss of adhesive property, suggesting that CD26 is a binding protein to the extracellular matrix. Moreover, our *in vitro* data indicate that humanized anti-CD26 mAb induces cell lysis of malignant mesothelioma cells via antibody-dependent cell-mediated cytotoxicity in addition to its direct anti-tumor effect via $p27^{kip1}$ accumulation. *In vivo* experiments with mouse xenograft models involving human malignant mesothelioma cells show that humanized anti-CD26 mAb treatment drastically inhibits tumor growth in tumor-bearing mice, resulting in enhanced survival.

Conclusions: Our data strongly suggest that humanized anti-CD26 mAb treatment may have potential clinical use as a novel cancer therapeutic agent in CD26-positive malignant mesothelioma.

Malignant mesothelioma is an aggressive cancer arising from the mesothelial cells lining the pleura. It is usually associated with the history of chronic asbestos exposure (1). Because of the long latency period between asbestos exposure and tumor development, the annual incidence of 2,500 new cases in the United States is expected to increase by >50% in the coming decade (2). Moreover, incidence world wide is projected to increase substantially in the next decades (3). The prognosis is very poor with a median survival of 4 to 12 months despite the therapies currently used, inducing surgery, radiotherapy, and chemotherapy (4). Because of the inefficacy of the conventional treatments, novel therapeutic strategies are urgently needed to be developed.

CD26 is a 110-kDa surface glycoprotein with dipeptidyl peptidase IV activity able to cleave selected biological factors to alter their functions (5). CD26/dipeptidyl peptidase IV is involved in T-lymphocyte costimulation and signal transduction processes (6, 7) and regulates topoisomerase II α level in hematologic malignancies, affecting sensitivity to doxorubicin and etoposide (8). Expressed on various tissues (4, 9), CD26 is involved in the development of certain human cancers (9–12). CD26 is also known to serve as a binding motif for extracellular matrix (ECM) in human and rodents (13, 14). Previously, we reported that CD26 was collagen-binding protein using a CD26 positive JMN cell line, which is derived from malignant mesothelioma (15). Moreover, our previous works have shown that anti-CD26 monoclonal antibody (mAb) inhibits growth of CD26-positive T-cell malignancies (16, 17) and renal cell carcinoma (18).

Authors' Affiliations: [1]Division of Clinical Immunology, Advanced Clinical Research Center, Institute of Medical Science, University of Tokyo and [2]Department of Pathology, Keio University, Tokyo, Japan; [3]Department of Medicine, Osaka Medical College, Osaka, Japan; and [4]Department of Hematologic Malignancies, Nevada Cancer Institute, Las Vegas, Nevada

Received 1/16/07; revised 3/14/07; accepted 3/22/07.

Grant support: Ministry of Education, Science, Sports, and Culture grant (K. Ohnuma and C. Morimoto), Ministry of Health, Labor, and Welfare, Japan (C. Morimoto), and Yasuda Medical Foundation (T. Inamoto).

The costs of publication of this article were defrayed in part by the payment of page charges. This article must therefore be hereby marked *advertisement* in accordance with 18 U.S.C. Section 1734 solely to indicate this fact.

Conflict of interest: Dr. Morimoto is a board member of Y's Therapeutics, and Dr. Dang is a scientific adviser in Y's Therapeutics. The other authors have no competing financial interests.

Requests for reprints: Chikao Morimoto, Division of Clinical Immunology, Advanced Clinical Research Center, Institute of Medical Science, University of Tokyo, 4-6-1, Shirokanedai, Minato-ku, Tokyo 108-8639, Japan. E-mail: morimoto@ims.u-tokyo.ac.jp.

doi:10.1158/1078-0432.CCR-07-0110

Our previous report shows that the murine anti-CD26 mAb 14D10, which recognizes the cell membrane-proximal glycosylated region starting with a 20-amino acid flexible stalk region of human CD26, has direct antitumor effect by inducing G_1-S arrest while concomitantly blocking the adhesion of cancer cells to the ECM. However, another murine anti-CD26 mAb, termed 5F8, which detects the cysteine-rich domain of CD26, lacks this biological activity (18).

Because human malignant mesothelioma is a highly malignant tumor resistant to apparent conventional treatment, the detection of novel target and development of new treatment strategies in malignant mesothelioma are urgently needed (4, 19). In this report, we analyzed the expression of CD26 in the tissues of patients with malignant mesothelioma and validated the antitumor effect of a novel humanized anti-CD26 mAb which was constructed from high-affinity Fab clone to the 14D10 variable region by targeting malignant mesothelioma, hence concomitantly showing the functional role of CD26 in this neoplasm.

Materials and Methods

Reagents and antibodies. Anti-CD26 mouse mAb (IgG1)14D10, 5F8, and anti-CD45RA mouse mAb (IgG1) 2H4 were developed in our laboratory as described previously (20, 21), with the last one being used as control. Normal human IgG1 (Sigma-Aldrich) was also used as a control. Humanized anti-CD26 mAb (IgG1 isotype) was constructed from 14D10 coding sequence (generously provided by Y's Therapeutics). Mouse mAb to PKBα/Akt, CDK2, CDK4, CDK6, cyclin E, and β-actin were from Cell Signaling Technology Inc., and mouse mAb to $p27^{kip1}$, $p21^{cip1/waf1}$, cyclin D1, and activated caspase-3 were from BD PharMingen. Antihuman IgG, Fcγ fragment specific F(ab')2 fragment of goat and anti-mouse IgG, Fcγ fragment specific F(ab')2 fragment of goat were from Jackson ImmunoResearch.

Cell culture and transfection. JMN cells were a kind gift from Dr. Brenda Gerwin (Laboratory of Human Carcinogenesis, NIH, Bethesda, MD). NCI-H2452 and 293T cells were obtained from the American Type Culture Collection. JMN and NCI-H2452 cell lines were derived from patients with malignant mesothelioma. All cells were grown in RPMI medium (Life Technologies Inc.) supplemented with 10% heat-inactivated fetal bovine serum, penicillin (100 units/mL), and streptomycin (100 μg/mL; Life Technologies) or G418 (500 μg/mL; Sigma-Aldrich). 293T cells were transfected with full-length CD26 subcloned into a pEB6 vector (22) using FuGENE6 reagent (Roche Diagnostics).

2-(2-methoxy-4-nitrophenyl)-3-(4-nitrophenyl)-5-(2,4-disulfophenyl)-2H-tetrazolium assay. Cells were subjected to incubation in 96-well plates in media alone or in the presence of humanized anti-CD26 mAb (0.1, 1.0, or 10 μg/mL) or 2H4 (0.1, 1.0, or 10 μg/mL) for a total volume of 100 μL (5×10^3 cells per well). After 24 h of incubation in 37°C, 2-(2-methoxy-4-nitrophenyl)-3-(4-nitrophenyl)-5-(2,4-disulfophenyl)-2H-tetrazolium (Seikagaku) was added to each well. After another 2 h of incubation, water soluble formazan dye upon bioreduction in the presence of an electron carrier, 1-methoxy-5-methylphenazinium, was measured at 450 nm using a microplate reader (Bio-Rad). All samples were tested in triplicate. Values reported represent the means of triplicated wells, and SE was within 15.

Immunohistochemistry. For immunohistochemistry, 12 patients' surgical specimens consisting of seven malignant mesothelioma, three reactive mesothelial cells, and two adenomatoid tumors were evaluated. For each, 10% formalin-fixed, paraffin-embedded specimens, containing both the carcinoma and its adjacent nonneoplastic tissue, were prepared. Paraffin-embedded tissues were dewaxed and rehydrated using xylene and ethanol, respectively. Slides were deparaffinized, then heated in a microwave processor for antigen retrieval in 10 mmol/L citrate buffer (pH 6.0) for 10 min. After blocking in 3% (v/v) bovine serum albumin, slides were incubated at 4°C overnight with the primary antibody (anti-CD26 mAb) and washed with PBS and the secondary antibody was labeled with biotin and applied for 30 min. Streptavidin-LSA amplification method was carried out for 30 min followed by peroxidase/diaminobenzidine substrate/chromagen. The slides were counterstained with hematoxylin. Two different pathologists checked the validity of the obtained results. All human specimens were obtained from Department of Pathology, Keio University (Tokyo, Japan), and informed consents were obtained from all patients according to the format of the institutional review board.

Depletion of endogenous CD26. To deplete endogenous CD26, small interfering RNA (siRNA) oligo-targeting CD26 cDNA (accession no. NM_001935) was made according to the design site of TAKARA BIO;[5] sense: 5'-GAAAGGUGUCAGUACUAUU TT-3', antisense: 3'-TT CUUUCCACAGUCAUGAUAA-5', with scrambled control of small interfering RNA oligo-targeting human Cas-L; sense: 5'-UAAUUAGG-GUCGGGUAAAC TT-3', antisense: 3'-TT AUUAAUCCCAGCCCA-UUUG-5' being used as control. CD26 siRNA oligo (siCD26) was transfected using TransIT-TKO transfection reagent (Mirus Bio Corporation) according to the manufacturer's protocol.

SDS-PAGE and immuno-blotting. Preparation of whole-cell lysates, cell fractionations, and SDS-PAGE were done as described elsewhere (23).

Antibody-dependent cell-mediated cytotoxicity. The capacity of mAb to induce effector cell-dependent lysis of tumor cells was evaluated in Calcein-AM-release assay. Healthy donor natural killer cells were isolated from peripheral blood mononuclear cells by NK Cell Isolation kit II Miltenyi Biotec (Bergisch Gladbach) and used as effector cells. Target cells (1×10^6) were labeled with 10 μmol/L Calcein-AM (Dojindo) under shaking conditions at 37°C for 1 h. Cells were washed thrice with PBS and were resuspended in culture medium (1×10^5 cells/mL). Labeled cells were dispensed in 96-well U-bottomed plates (5×10^3 in 50 μL/well) and preincubated (37°C, 30 min) with 50 μL of 7-fold serial dilutions of humanized anti-CD26 mAb or 14D10 in culture medium, ranging from 0.1 pg/mL to 0.1 mg/mL (final concentrations). Culture medium was added instead of mAb to determine the spontaneous Calcein-AM release, with Triton X-100 (1% final concentration) being added to determine the maximal Calcein-AM release. Thereafter, human effector cells (HuEC) were added to the wells (5×10^5 cells per well) and cells were incubated at 37°C overnight. Supernatants were then collected for measurement of the Calcein-AM release. Percentage of specific lysis was calculated using the following formula: % specific lysis = (experimental release - spontaneous release)/(maximal release - spontaneous release) × 100; where maximal release was determined by adding Triton X-100 to target cells and spontaneous release was measured in the absence of sensitizing Abs and effector cells.

Complement-dependent cytotoxicity. Complement-dependent cytotoxicity (CDC) assay was done as described previously (24). Target cells were dispensed in 96-well U-bottomed plates (1×10^5 cells per well) incubated with various concentrations of mAbs at 4°C for 30 min. Subsequently, human serum was added and cells were incubated at 37°C for 2 h. Evaluation of CDC-specific cell death along with antibody-dependent cell-mediated cytotoxicity (ADCC)-specific cell death was assessed by Annexin V-FITC Apoptosis Detection kit (BioVision) and detection of activated caspase-3.

Assessment of antitumor activity of humanized anti-CD26 mAb in effector-depleted SCID mice. All *in vivo* studies were approved by the Institute Animal Care and Use Committee. Six-week-old female NOD-SCID mice were purchased from Charles River (Kanagawa, Japan) and were pretreated with anti-asialo-GM1 polyclonal antisera 25% (v/v; WAKO) i.p. 1 day before mAb treatment.

[5] http://www.takara-bio.co.jp/RNAi.htm

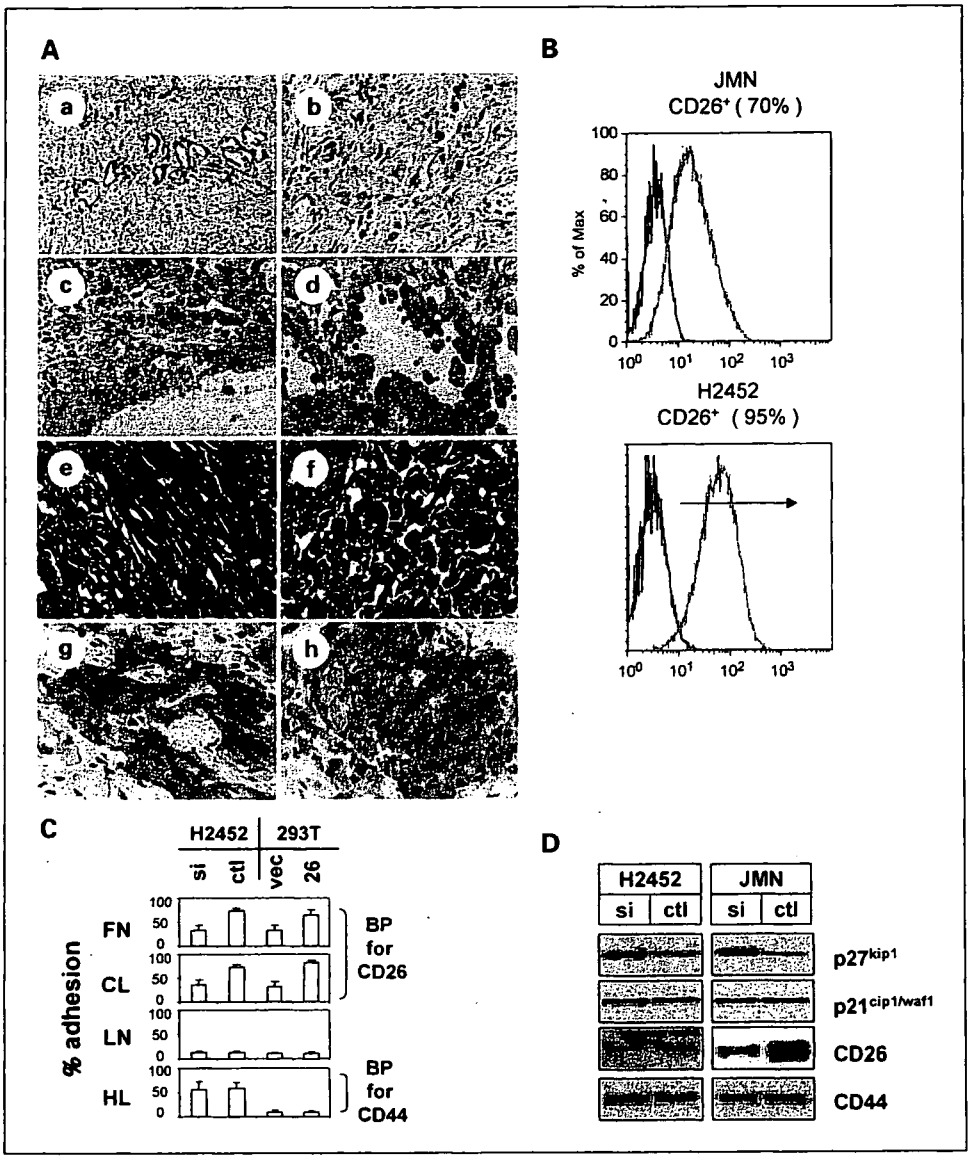

Fig. 1. Expression and functional role of CD26 in malignant mesothelioma. *A*, immunochemical localization of CD26 in adenomatoid tumor, reactive mesothelial cells and malignant mesothelioma. *a*, CD26 in adenomatoid tumor; *b*, CD26 in reactive mesothelial cells; *c*, CD26 in localized malignant mesothelioma; *d*, CD26 in well-differentiated papillary malignant mesothelioma; *e* and *f*, H&E stain in diffuse malignant mesothelioma; *g and h*, CD26 in diffuse malignant mesothelioma. Diffuse malignant mesothelioma specimens are showing biphasic features of sarcomatous malignant mesothelioma (*f, h*) and epithelial malignant mesothelioma (*g, i*). Indicated panels are representative of 12 consecutive specimens. Original magnification, ×100. *B*, surface expression of CD26 on mesothelioma cell lines was analyzed by flow cytometry. Gray line, CD26 histograms were obtained by staining mouse anti-CD26mAb (14D10) followed by staining with rabbit anti-mouse Igb FITC conjugate; black line, control histograms represent back ground fluorescence obtained by staining of isotype-matched control mAb (2H4). *C*, adhesive property of CD26 to ECM. CD26-depleted NCI-H2452 (*si*), scrambled control oligo-transfected NCI-H2452 (*ctl*), pEB6 vector – transfected 293T (*vec*), or pEB6-CD26 – transfected 293T (26) were plated onto 60-mm dishes (2×10^6 cells per dish) coated with fibronectin (*FN*), collagen I (*CL*), laminin (*LN*), or hyaluronan (*HL*) and cultured for 18 h. Fibronectin and collagen I are binding proteins (*BP*) to extracellular region of CD26, with hyaluronan being binding protein for CD44. The adhesive ability of cancer cells was expressed as the mean number of cells that had attached to the bottom surface of the dish. Columns, number of cells per field of view; bars, SD. Values for adhesion were determined by calculating the average number of adhesive cells per squared millimeters over three fields per assay and expressed as an average of triplicate determinations. Adhesive cells (%): adhesive cells/adhesive cells + nonadhesive cells. *D*, depletion of CD26 elicits up-regulation of $p27^{kip1}$. NCI-H2452 cells and JMN cells were transfected with siRNA oligo (*si*) of CD26 or control oligo (*ctl*). At 48 h after transfection, cells were harvested, lysed, and subjected to SDS-PAGE, then probed by specific antibody to $p27^{kip1}$, $p21^{cip1/waf1}$, CD26, and CD44.

To assess the effect of humanized anti-CD26 mAb against tumorigenicity, JMN cells (1×10^6) were inoculated s.c. into the left flank of mice. Mice were treated with intratumoral injection of isotype-matched control mAb and 5F8, 14D10, or humanized anti-CD26 mAb (10 μg per each injection) on the 14th day after cancer cell inoculation when the tumor mass became visible (5 mm in size). Each mAb was given thrice per week. Tumor-bearing mice were then monitored for tumor development and progression. Tumor size was determined by caliper measurement of the largest (x) and smallest (y) perpendicular diameters and was calculated according to the formula $V = \pi/6 \times xy^2$.

To assess the effect of humanized anti-CD26 mAb against tumor dissemination, JMN cells (1×10^5) were injected i.v. via tail vein. Thereafter, mice were treated with i.v. injection of isotype-matched control mAb and 5F8, 14D10, or humanized anti-CD26 mAb (10 μg per each injection), starting on the day of cancer cell injection. Each mAb was given thrice per week. Cumulative proportion survival was assessed by Kaplan-Meier.

Table 1. CD26 expression profile in patient samples

Patient no.	Gender/Age	Origin	Histology	CD26	
				CS	C
1	M/55	Pleura	RMC	-	±
2	F/63	Pleura	RMC	-	±
3	M/58	Pleura	RMC	-	±
4	F/39	Ovary	AT	-	+
5	F/5	Ovary	AT	-	±
6	M/67	Pleura	MM	+	++
7	M/60	Pleura	MM	++	+++
8	M/49	Pleura	MM	+	++
9	F/74	Pleura	MM	-	++
10	M/50	Pleura	MM	++	++
11	M/77	Pleura	MM	+	+++
12	M/61	Pleura	MM	+	+++

Abbreviations: RMC, reactive mesothelial cell; AT, adenomatoid tumor; MM, malignant mesothelioma; CS, cell surface; C, cytoplasm.

Assessment of antitumor activity of humanized anti-CD26 mAb in effector-present Balb mice. Six-week-old female Balb mice were purchased from Charles River, and treatment with anti-asialo-GM1 polyclonal antisera was not introduced to preserve the binding of the mouse effector system.

To assess the effect of humanized anti-CD26 mAb against tumorigenicity, JMN cells (1×10^6) were inoculated s.c. into the left flank of mice. Mice were treated with intratumoral injection of isotype-matched control mAb and 5F8, 14D10, or humanized anti-CD26 mAb (10 μg per each injection) on the 14th day after cancer cell inoculation when the tumor mass became visible (5 mm in size). Each mAb was given thrice per week. Tumor-bearing mice were then monitored for tumor development and progression. Tumor size was determined by caliper measurement of the largest (x) and smallest (y) perpendicular diameters and was calculated according to the formula $V = \pi/6 \times xy^2$. On the 35th day after the first mAb treatment, all mice were euthanized to assess the microscopic feature of resected specimens in s.c. tumorigenicity model.

To assess the effect of humanized anti-CD26 mAb against tumor dissemination, JMN cells (1×10^5) were i.v. injected via tail vein. Thereafter, mice were treated with i.v. injection of isotype-matched control mAb or humanized anti-CD26 mAb (10 μg per each injection) starting on the day of cancer cell injection. Each mAb was given thrice per week. Cumulative proportion of survival was assessed by Kaplan-Meier. To further assess the effect of humanized anti-CD26 mAb on distant metastasis formation, treated mice were euthanized and multiple metastasis formation in the lung and liver was calculated in another tumor dissemination model. JMN cells (1×10^5) were injected i.v. into mice in each group. Mice were treated with i.v. injection of isotype-matched control mAb (lane 1, $n = 4$), 5F8 (lane 2, $n = 4$), 14D10 (lane 3, $n = 4$), or humanized anti-CD26 mAb (lane 4, $n = 4$) on the day of cancer cell injection. Each mAb was given thrice per week. On the 35th day after cancer cell injection, mice were euthanized and multiple metastasis formation in the lung and liver was calculated.

Construction of HuEC-engrafted mice and assessment of antitumor activity in NOD/Shi-scid. IL-Rγ^{null} mice. NOD/Shi-scid. IL-Rγ^{null} (NOG mice) were obtained from Central Institute for Experimental Animals. Human peripheral blood mononuclear cells were isolated from the peripheral blood of a healthy donor using Lymphoprep (AXIS-SHIELD) and were used as HuEC. Thereafter, HuEC (5×10^6 cells) were injected i.p. in a volume of 0.2 mL suspended in PBS into NOG-SCID mice under sterile conditions. The mice were pretreated with a 0.2 mL anti-asialo-GM1 polyclonal antisera 25% (v/v; WAKO) given i.p. 1 day before HuEC injection. NCI-H2452 cells (5×10^4) were injected i.p. into SCID mice engrafted with human HuEC 1 day after HuEC injection. One, three, and five days later, humanized anti-CD26 mAb were injected i.p. Mice were observed daily to monitor for death due to ascites tumor development. Cumulative proportion of survival was assessed by Kaplan-Meier.

Results

Cell surface CD26 is highly expressed on human malignant mesothelioma. We first evaluated CD26 expression level on surgically resected human malignant mesothelioma tissues from patients. Twelve consecutive surgically resected specimens from the primary sites were examined for cell surface CD26 expression. CD26 was highly expressed on all malignant mesothelioma tissues (Fig. 1A; Table 1). In adenomatoid tumor or reactive mesothelial cells, CD26 expression was very weak (Fig. 1A-a,b). In contrast, CD26 was highly expressed in various pathologic types of malignant mesothelioma, including localized malignant mesothelioma, well-differentiated papillary malignant mesothelioma, and diffuse malignant mesothelioma (Fig. 1A-c to h). These results suggested that CD26 is highly expressed in malignant mesothelioma but not in benign mesothelial tissues.

CD26 plays a role in cell adhesion to ECM. Malignant mesothelioma cell lines, JMN and NCI-H2452, exhibited high-surface CD26 expressions (Fig. 1B).

Because CD26 has been described previously to play a role in cell adhesion to the ECM proteins (13, 25), we examined whether CD26 plays a role in cellular interaction with the ECM. As seen in Fig. 1C, NCI-H2452 that were depleted of endogenous CD26 using siRNA oligo showed significant loss of CD26 binding to ECM proteins, including fibronectin and collagen I. In contrast to these results, depletion of CD26 did not alter binding to laminin (an ECM protein lacking binding ability to CD26) or hyaluronan (a ligand for CD44; Fig. 1C). In further support of these findings, 293T cells transfected with full-length CD26 cDNA subcloned into pEB6 vector showed higher binding ability to fibronectin and collagen I than control pEB6-transfected 293T cells (Fig. 1C). Moreover, depletion of CD26 was associated with the up-regulation of $p27^{kip1}$ (Fig. 1D). These findings thus suggested that CD26 serves as a binding molecule to distinct ECM proteins and that contact inhibition may play a contributing role to the observed CD26 depletion-mediated up-regulation of $p27^{kip1}$ associated with CD26 depletion (26, 27).

Anti-CD26 mAb perturbs cellular binding to ECM. Because CD26 proved to be an ECM-binding protein, we further evaluated whether anti-CD26 mAbs disrupt cellular adhesion to ECM. For this purpose, isotype-matched control mAb and 5F8, 14D10, and humanized anti-CD26 mAb were evaluated for potential disruption to cellular adhesion to ECM. As seen in Fig. 2A, JMN cells treated with 14D10 and humanized anti-CD26 mAb had decreased binding to fibronectin and collagen I, whereas control mAb and 5F8 (anti-CD26 mAb without biological function) did not influence binding to fibronectin and collagen I. Moreover, 14D10 and humanized anti-CD26 mAb transmitted direct growth inhibition to JMN cells by *in vitro* proliferation assay in a dose-dependent manner, with humanized anti-CD26 mAb having a stronger antiproliferative

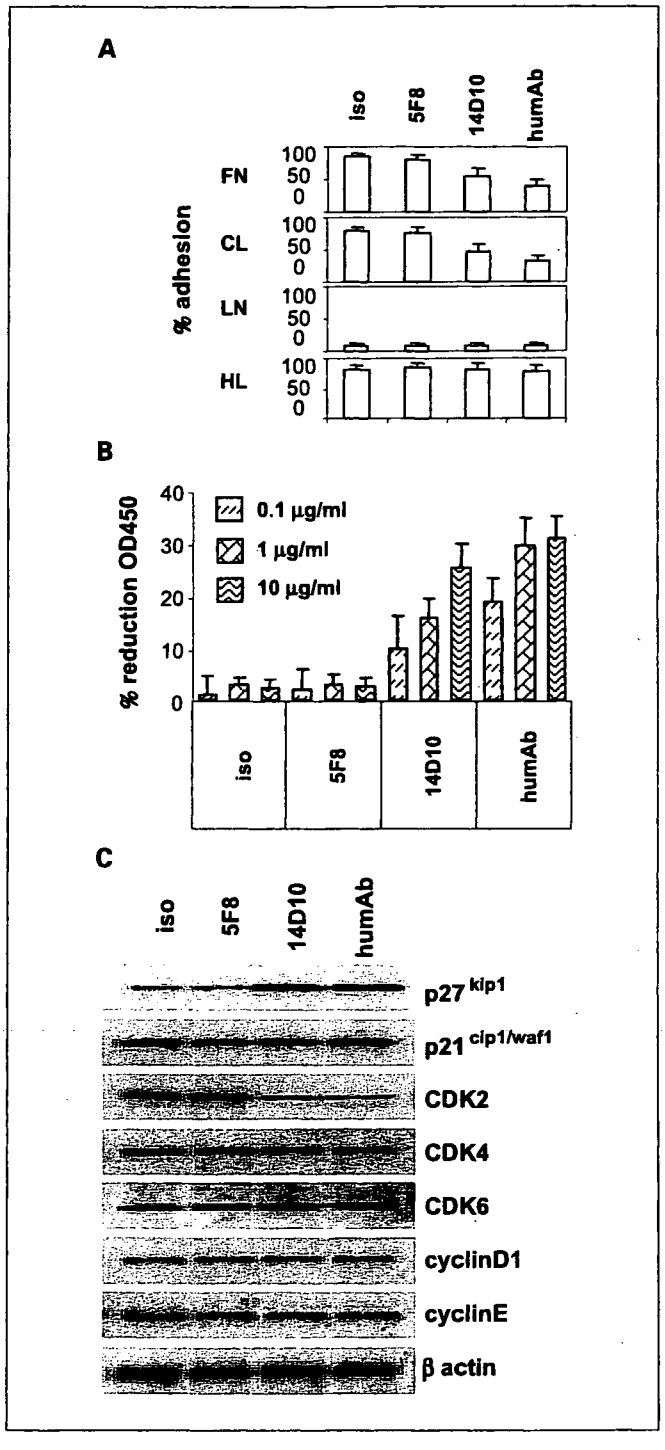

Fig. 2. Inhibitory effect of anti-CD26 mAbs on malignant mesothelioma proliferation. *A*, effect of anti-CD26 mAb on cell adhesion to ECM. JMN cells treated with isotype-matched control mAb (*iso*), 5F8, 14D10, or humanized anti-CD26 mAb (*humAb*) were plated onto 60-mm dishes (2×10^6 cells per dish) coated with fibronectin, collagen I, laminin, or hyaluronan and cultured for 18 h. Adhesive cells (%): adhesive cells/adhesive cells + nonadhesive cells. *B*, 5×10^3 cells per well of JMN were incubated in 96-well plates in the presence of either isotype-matched control mAb, 5F8, 14D10, or humanized anti-CD26 mAb. After 24 h of antibody treatment, water-soluble formazan dye upon bioreduction in the presence of an electron carrier, 1-methoxy-5-methylphenazinium, was measured at 450 nm using a microplate reader as described in Materials and Methods, and growth inhibitory ratio was calculated as percentage reduction of absorbance 450 nm. *C*, JMN cells were treated with isotype-matched control mAb, 5F8, 14D10, or humanized anti-CD26 mAb. At 18 h after antibody administration, cells were harvested, lysed, and subjected to SDS-PAGE, then probed by specific antibody to $p27^{kip1}$, $p21^{cip1/waf1}$, CDK2, CDK4, CDK6, cyclinD1, cyclinE, and β-actin.

effect than 14D10 (Fig. 2B). Importantly, 14D10 and humanized anti-CD26 mAb induced up-regulation of $p27^{kip1}$ and down-regulation of CDK2. These results suggested that both 14D10 and humanized anti-CD26 mAb dynamically transmit contact inhibition–related growth inhibition via up-regulation of $p27^{kip1}$ and down-regulation of CDK2.

Humanization of anti-CD26 mAb results in ADCC. Whereas both 14D10 and humanized anti-CD26 mAb had similar direct effect on cancer cells, our present studies emphasized the different biological effects of humanized anti-CD26 mAb compared with 14D10 through the use of ADCC assay with HuEC. When effector/target (E/T) ratio was held constant at 50, JMN cells treated with humanized anti-CD26 mAb showed specific lysis via ADCC in an antibody dose-dependent manner (Fig. 3A, left). Importantly, JMN cells treated with 14D10 did not show ADCC-specific lysis (Fig. 3A, left), suggesting that humanization of 14D10 to humanized anti-CD26 mAb results in the induction of potent ADCC activity via engagement of the human effector system. Moreover, as seen in Fig. 3A (right), humanized anti-CD26 mAb provoked ADCC-specific lysis in effector-dose–dependent manner. These results were also found when other CD26 positive malignant mesothelioma line besides JMN (NCI-H2452) was used as target cells (Table 2). These data suggested that humanized anti-CD26 mAb possesses a novel biological function other than the direct effect on target cells seen with 14D10, namely ADCC-specific lysis. To better characterize the humanized anti-CD26 mAb–mediated ADCC, apoptosis assays using propidium iodide–annexin V staining and detection of cleaved caspase-3 were used. In these assays, cross-linking method using anti-human IgG, Fcγ fragment specific F(ab')2 fragment of goat, and anti-mouse IgG, Fcγ fragment specific F(ab')2 fragment of goat were used as mimicry of human effectors to humanized anti-CD26 mAb and 14D10, respectively. As seen in Fig. 3B (top three panels), cross-linked humanized anti-CD26 mAb induced late apoptosis, whereas cross-linked 14D10 did not induce late and early apoptosis. Importantly, neither humanized anti-CD26 mAb nor 14D10-induced CDC using human complement (Fig. 3B). To further support these binding, only cross-linked humanized anti-CD26 mAb induced activation of caspase-3 in JMN cells, whereas neither cross-linked 14D10, humanized anti-CD26 mAb plus human complement, and 14D10 plus human complement induced activation of caspase-3 (Fig. 3C). These results therefore indicated that humanized anti-CD26 mAb elicits ADCC-specific lysis but not CDC-specific lysis.

Humanized anti-CD26 mAb possesses direct in vivo antitumor effect on malignant mesothelioma cells. Because we recently showed that 14D10 exhibits direct *in vivo* antitumor effect on solid tumors (24), we further examined whether humanized anti-CD26 mAb has similar *in vivo* antitumor effect. For this purpose, we used NOD-SCID mice, which lack functional B and T cells as well as most natural killer cell activity (28). To minimize the effect of mouse effector cells, NOD-SCID mice were pretreated by anti–asialo-GM1 polyclonal antisera before being subjected to humanized anti-CD26 mAb functional evaluation. As seen in Fig. 4A and B, humanized anti-CD26 mAb and 14D10 reduced the tumorigenicity of s.c. inoculated JMN, with humanized anti-CD26 mAb being more potent in reducing tumor formation. These observed results suggested that humanized anti-CD26 mAb possesses stronger direct antitumor effect than 14D10. To

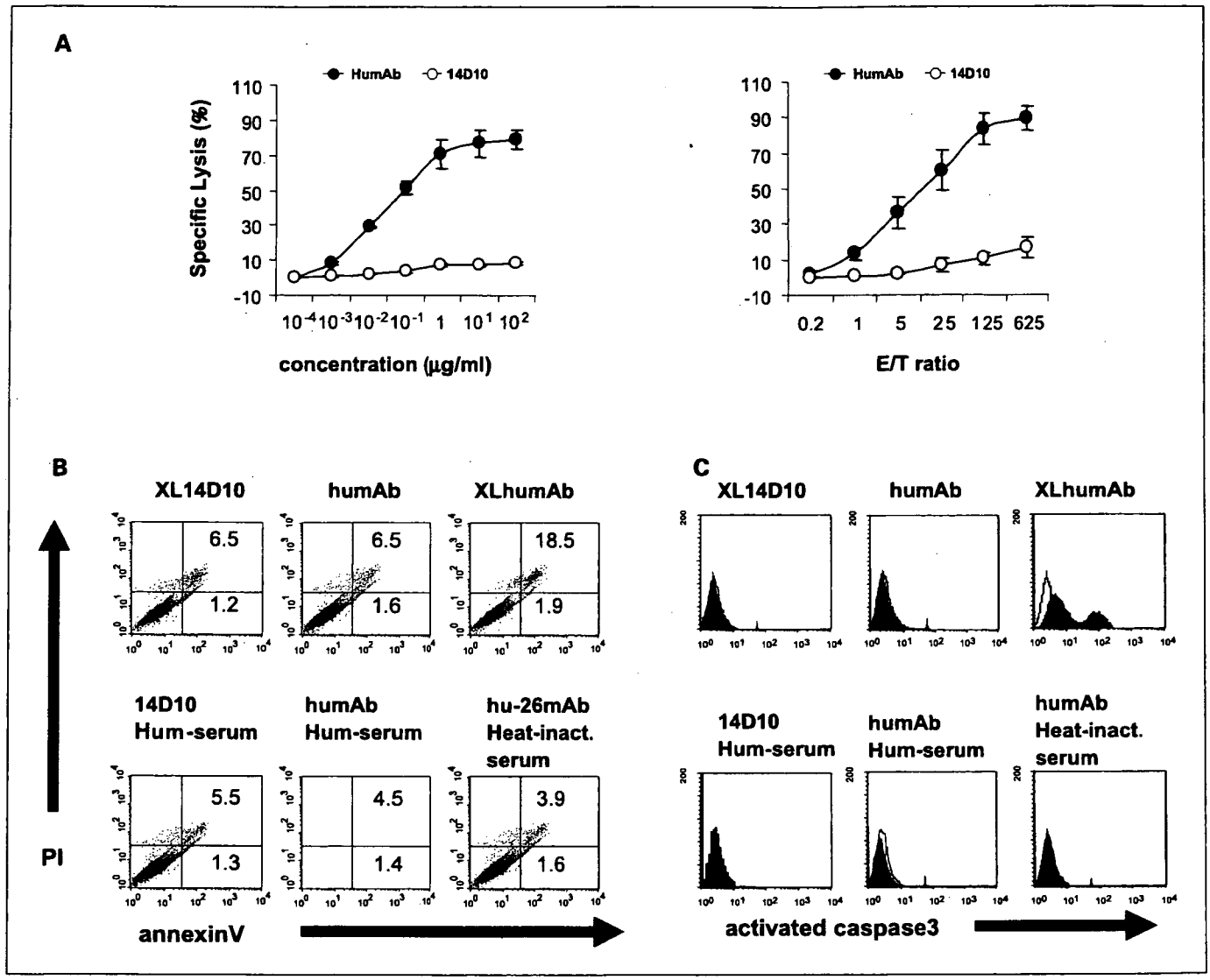

Fig. 3. ADCC-specific lysis of JMN cells by humanized anti-CD26 mAb. *A*, ADCC of humanized anti-CD26 mAb and 14D10 at the indicated concentrations on the *X* axis were examined (*left*). Effector/target (*E/T*) ratio was held constant at 50. ADCC of humanized anti-CD26 mAb and 14D10 in the presence of varying effector/target ratios were examined (*right*). Concentrations of mAbs were held constant at 5 μg/mL. Natural killer cells from healthy donor were used as effector cells. *B*, as a mimicry of effector cells in ADCC effects, cross-linking (*XL*) method of humanized anti-CD26 mAb and 14D10 was used. Top, cross-linked 14D10, intact humanized anti-CD26 mAb, cross-linked humanized anti-CD26 mAb, respectively. To examine the CDC, human serum was used. Bottom, 14D10 with serum, humanized anti-CD26 mAb with serum, and humanized anti-CD26 mAb with heat-inactivated serum. *X* axis, annexinV; *Y* axis, propidium iodide (*PI*). *C*, activated caspase-3 was evaluated in JMN cells pretreated with the cross-linked 14D10, intact humanized anti-CD26 mAb, cross-linked humanized anti-CD26 mAb, respectively (*top*), or in JMN cells pretreated with the 14D10 plus serum, humanized anti-CD26 mAb plus serum, and humanized anti-CD26 mAb plus heat-inactivated serum, respectively (*bottom*). X axis, activated caspase 3, Y axis, relative cell markers.

further examine the direct antitumor activity of humanized anti-CD26 mAb on tumor dissemination, we examined the effect of i.v.-given antibodies in a JMN xenograft model. As seen in Fig. 4C, humanized anti-CD26 mAb and 14D10 enhanced mouse survival when both antibodies were given i.v., with humanized anti-CD26 mAb being more efficient in promoting survival. All together, these observed results suggested that humanized anti-CD26 mAb is more potent than 14D10 in its direct antitumor activity.

Mouse effector system may potentiate antitumor effect of anti-CD26 mAb. While both humanized anti-CD26 mAb and 14D10 showed direct *in vivo* antitumor effect, we next examined the potential involvement of mouse effector system in anti-CD26 mAb activity induced antitumor effect. For this purpose, we used Balb mice which possess robust natural killer cell activity. As seen in Fig. 5A, humanized anti-CD26 mAb and 14D10 reduced the tumorigenicity of s.c.-inoculated JMN. It should be noted that both 14D10 and humanized anti-CD26 mAb reduced tumor formation in the presence of mouse effector system (Fig. 5A). As seen in Fig. 5B, both humanized anti-CD26 mAb and 14D10-treated tumors showed resultant dead tissues upon microscopic analyses. These results suggested that both humanized anti-CD26 mAb and 14D10 used the mouse effector system in marked contrast with the observed differences between humanized anti-CD26 mAb and 14D10 in a mouse effector-depleted xenograft model. Additional studies using i.v. administration of JMN cells showed that i.v. injection of humanized anti-CD26 mAb effectively enhanced mouse

Table 2. Specific lysis by humanized anti-CD26 mAb in human malignant mesothelioma lines

MFI	JMN	NCI-H2452
CD26	68	56
% ADCC lysis	67	65

Abbreviations: MFI, mean fluorescent intensity; % ADCC lysis, percentage of ADCC-specific lysis.

survival in the presence of mouse effector system (Fig. 5C). Importantly, formation of distant JMN was similarly inhibited by both humanized anti-CD26 mAb and 14D10 (Fig. 5D). These data indicated that mouse effector system potentiates the anti-CD26 mAb–mediated direct antitumor effect.

Human effector system may potentiate antitumor effect of humanized anti-CD26 mAb. We next evaluated the potential involvement of human effector system in anti-CD26 mAb induced antitumor effect. For this purpose, NOG mice which have significant defects in T, B, and natural killer cell activities were used in a NCI-H2452 xenograft model construction. Human peripheral blood mononuclear cells were used as HuEC in this *in vivo* model. To completely deplete mouse effector system, NOG mice were pretreated with anti–asialo-GM1 antisera 1 day before i.p. HuEC implantation. As seen in Fig. 6, i.p. administration of humanized anti-CD26 mAb drastically enhanced NCI-H2452 xenograft mouse survival in the absence of HuEC. It should be noted that while 14D10 also enhanced mouse survival, its effect was much weaker than humanized anti-CD26 mAb in the absence of HuEC (Fig. 6). These results suggested that humanized anti-CD26 mAb possesses stronger direct antitumor effect. Importantly, in the presence of HuEC, the antitumor effect of humanized anti-CD26 mAb was exaggerated, whereas the antitumor effect of 14D10 was not altered significantly (Fig. 6). All together these observed results suggested that CD26 is an appropriate molecular target for mesothelioma therapy and humanized anti-CD26 mAb regulates tumor growth by at least two distinct mechanisms of action through its direct antitumor activity, as well as its ability to engage human effector system.

Discussion

In this study, we show the antitumor effect of anti-CD26 mAb in an *in vitro* and *in vivo* model. Importantly, our study suggests that humanization of anti-CD26 mAb yields additive antitumor effect to contact inhibition associated with $p27^{kip1}$ induction. Our study also indicates the functional role of CD26 as a binding protein to ECM in human malignant mesothelioma.

Immunohistologic analysis indicates that human malignant mesothelioma cells express high level of surface CD26 than nonmalignant tissue, suggesting that CD26 may play a role in cancer growth and progression. It should be noted that depletion of endogenous CD26 in NCI-H2452 using siRNA oligo results in significant loss of binding to ECM, including fibronectin and collagen I. Moreover, 293T cells transfected with full-length CD26 cDNA exhibit higher binding affinity to fibronectin and collagen I than control mock-transfected 293T cells. Moreover, depletion of CD26 leads to the up-regulation of $p27^{kip1}$. These findings thus suggest that CD26 is involved in cancer cell adhesion to ECM and that contact inhibition may play a contributing role to the observed CD26 depletion–mediated up-regulation of $p27^{kip1}$. Of note is the fact that it has

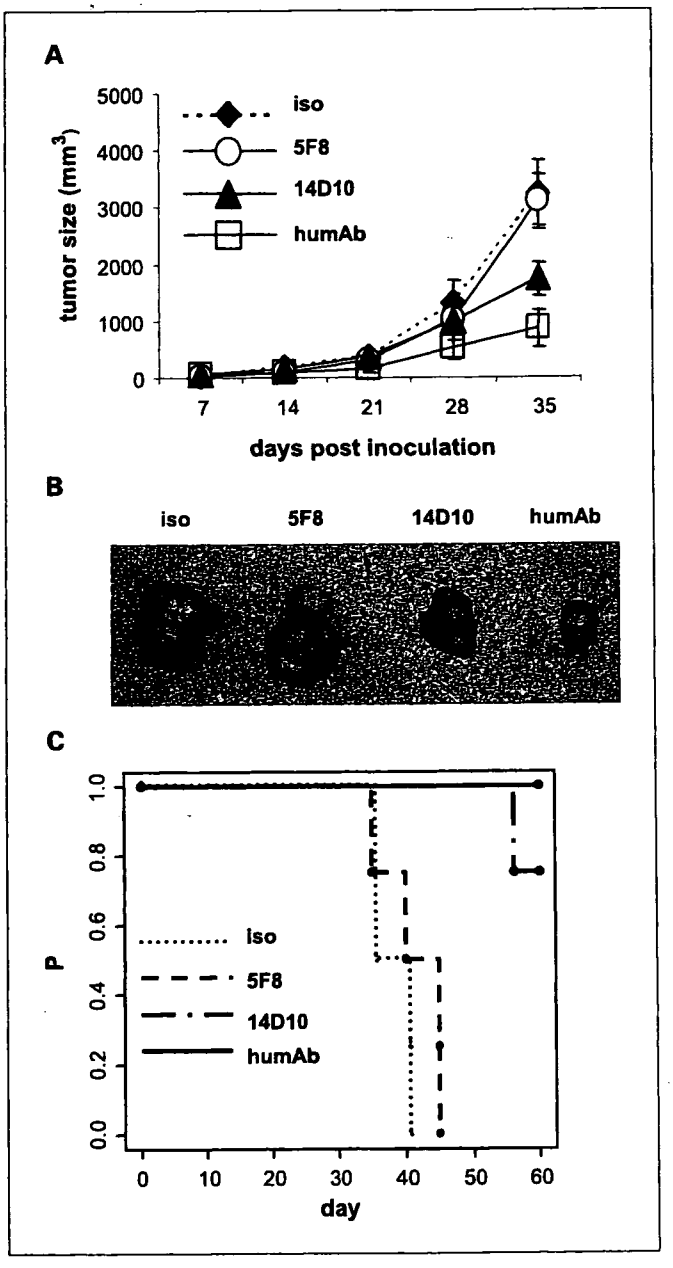

Fig. 4. *In vivo* direct effect of humanized anti-CD26 mAb: ADCC depletion model. Six-week-old female NOD-SCID mice were pretreated with anti–asialo-GM1 polyclonal antisera 1 d before treatment. *A*, effect of humanized anti-CD26 mAb in s.c. tumorigenicity was evaluated. JMN cells (1×10^6) were inoculated s.c. into the left flank of mice. Mice were treated with intratumoral injection of isotype-matched control mAb ($n = 4$), 5F8 ($n = 4$), 14D10 ($n = 4$), or humanized anti-CD26 mAb ($n = 4$) on the 14th day after cancer cell inoculation when the tumor mass became visible (5 mm in size). Each mAb was given at 10 μg per injection at thrice per week. *B*, representative resected specimens in s.c. tumorigenicity model on 35th day after first mAb treatment. *C*, effect of humanized anti-CD26 mAb in tumor dissemination model was evaluated. JMN cells (1×10^5) were injected i.v. into mice in each group. Mice were treated with i.v. injection of isotype-matched control mAb ($n = 4$), 5F8 ($n = 4$), 14D10 ($n = 4$), or humanized anti-CD26 mAb ($n = 4$) on the day of cancer cell injection. Each mAb was given at 10 μg per injection at thrice per week.

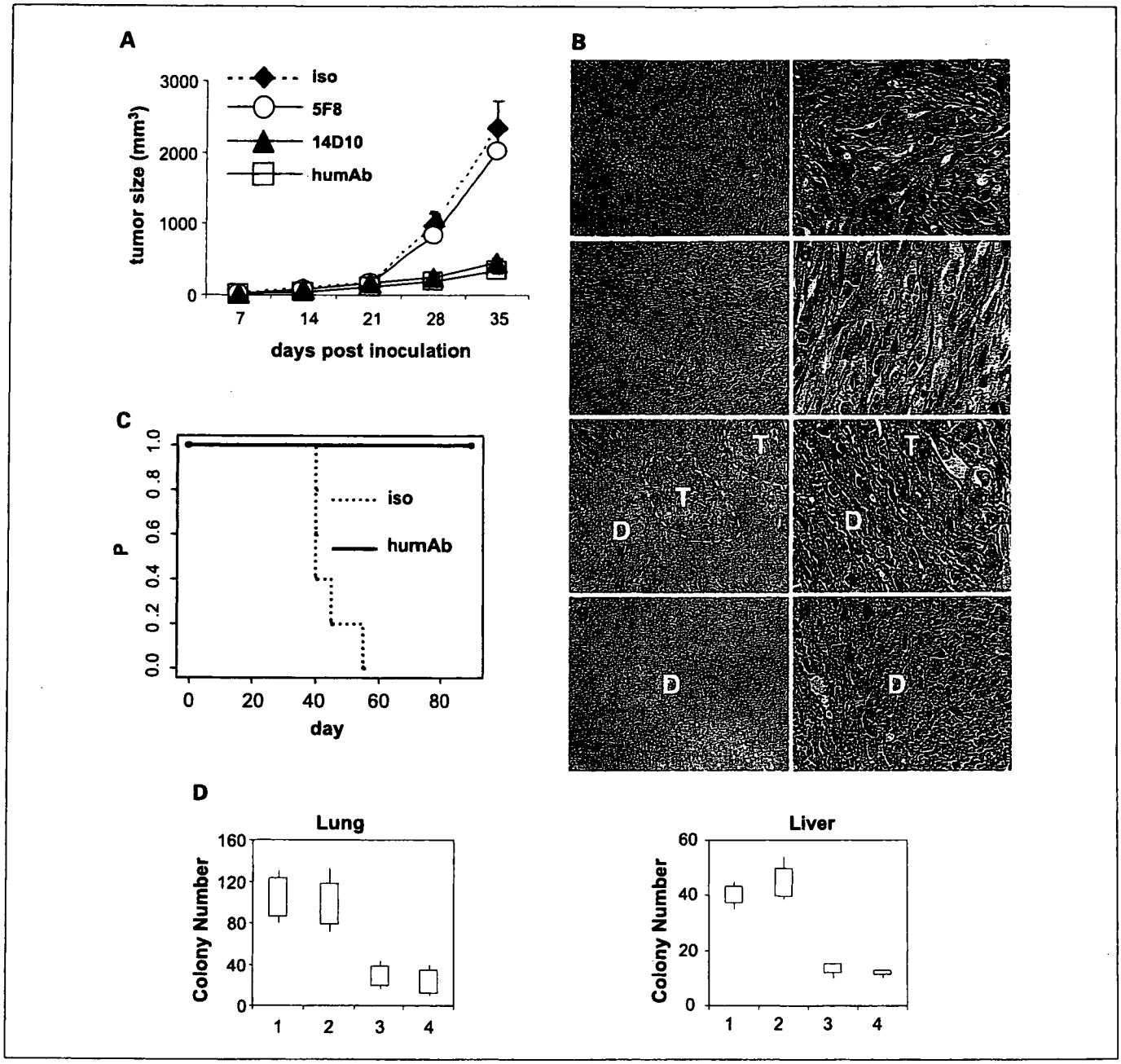

Fig. 5. *In vivo* direct and indirect effect of humanized anti-CD26 mAb: mouse ADCC presence model. Six-week-old female Balb mice were enrolled in this experiment. *A*, effect of humanized anti-CD26 mAb in s.c. tumorigenicity was evaluated. JMN cells (1×10^6) were inoculated s.c. into the left flank of mice. Mice were treated with intratumoral injection of isotype-matched control mAb ($n = 4$), 5F8 ($n = 4$), 14D10 ($n = 4$), or humanized anti-CD26 mAb ($n = 4$) on the 14th day after cancer cell inoculation when the tumor mass became visible (5 mm in size). Each mAb was given at 10 μg per injection at thrice per week. *B*, representative H&E stain feature of resected specimens in s.c. tumorigenicity model on 35th day after first mAb treatment. *a*, isotype-matched control mAb (×100); *b*, isotype-matched control mAb (×600); *c*, 5F8 (×100); *d*, 5F8 (×600); *e*, 14D10 (×100); *f*, 14D10 (×600); *g*, humanized anti-CD26 mAb (×100); *h*, humanized anti-CD26 mAb (×600). White broken line, the line between tumor (*T*) and dead tissue (*D*). *C*, effect of humanized anti-CD26 mAb in tumor dissemination model was evaluated. JMN cells (1×10^5) were injected i.v. into mice in each group. Mice were treated with i.v. injection of isotype-matched control mAb ($n = 5$) or humanized anti-CD26 mAb ($n = 5$) on the day of cancer cell injection. Each mAb was given at 10 μg per injection at thrice per week. *D*, effect of humanized anti-CD26 mAb onto distant metastasis formation in tumor dissemination model was evaluated. JMN cells (1×10^5) were injected i.v. into mice in each group. Mice were treated with i.v injection of isotype-matched control mAb (*lane 1*, $n = 4$), 5F8 (*lane 2*, $n = 4$), 14D10 (*lane 3*, $n = 4$), or humanized anti-CD26 mAb (*lane 4*, $n = 4$) on the day of cancer cell injection. Each mAb was given at 10 μg per injection at thrice per week. On 35th day after cancer cell injection, mice were euthanized and multiple metastasis formation in the lung and liver was calculated.

been previously reported that $p27^{kip1}$ is up-regulated during contact inhibition (26).

Both humanized anti-CD26 mAb and 14D10 display direct inhibition of malignant mesothelioma growth via $p27^{kip1}$ up-regulation and disruption of binding to ECM. Hence, our results with these anti-CD26 monoclonal antibodies are consistent with those obtained from above small interfering RNA study, showing that both humanized anti-CD26 mAb and 14D10 have an antagonistic effect on the adhesive property of malignant mesothelioma.

Further examination of their effector functions associated with anti-CD26 mAb–mediated antitumor effect indicates that humanized anti-CD26 mAb, but 14D10, elicits ADCC-induced cell lysis. Cross-linking of humanized anti-CD26 mAb results in an accumulation of annexin V–positive and propidium iodide–positive population and cleavage of activated caspase-3. These data suggest that humanization of anti-CD26 mAb elicits greater contribution from ADCC in addition to a direct antitumor effect. Meanwhile, the precious reason why humanized anti-CD26 mAb does not induce CDC activity is not clear at the moment. One of the reasons is the high-surface expression of DAF and CD59, which are antagonistic to human complement proteins (data not shown). Or, our *in vitro* system may not be appropriate for the induction of CDC activation.

In vivo study with NOD-SCID mice shows that humanized anti-CD26 mAb and 14D10 reduce the tumorigenicity of s.c.-inoculated JMN cells, suggesting that humanized anti-CD26 mAb possesses direct antitumor effect as well. Our results also suggest that humanized anti-CD26 mAb is more potent in reducing tumor formation, possibly due to its higher binding affinity to CD26 than 14D10.

Meanwhile, *in vivo* study with Balb mice show that humanized anti-CD26 mAb and 14D10 are equally effective in reducing the tumorigenicity of s.c.-inoculated JMN cells. These data suggest that the mouse effector system may potentiate the antitumor effect of 14D10 more than humanized anti-CD26 mAb. In fact, not only humanized anti-CD26 mAb but also 14D10-treated tumor specimens from these mice exhibit a reduction of viable cells in tumor mass. It is also noteworthy that both humanized anti-CD26 mAb and 14D10 reduce the formation of distant metastasis, findings which may be partly explained from our *in vitro* results that CD26 serves as a binding protein to distinct ECM proteins.

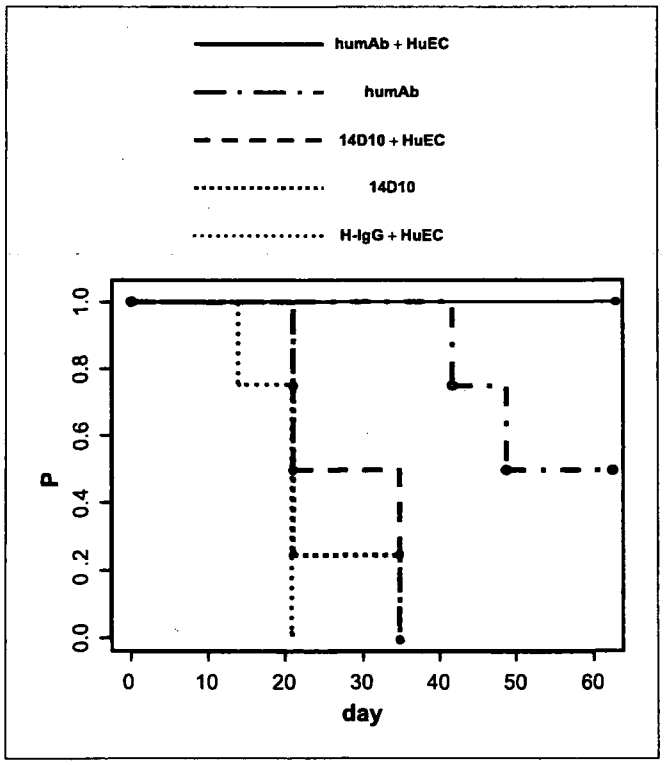

Fig. 6. *In vivo* direct and indirect effect of humanized anti-CD26 mAb: human ADCC presence model. Six-week-old female NOG-SCID mice were enrolled in this experiment. Mice were divided into two groups, HuECs-implanted group and HuEC-negative group, respectively. All mice were pretreated with anti – asialo-GM1 polyclonal antisera i.p. 2 d before HuEC implantation. HuEC were implanted i.p. with effector/target ratio of 10:1. JMN cells (1×10^6) were implanted 1 d after HuEC implantation into the peritoneal cavity of mice. The latter group was left untreated. All mice were treated with human normal IgG + HuEC (*H-IgG+HuEC*, $n = 4$), 14D10 ($n = 4$), 14D10 + HuEC ($n = 4$), humanized anti-CD26 mAb ($n = 4$), or humanized anti-CD26 mAb+HuEC (*humAb+HuEC*, $n = 4$). Each mAb was given i.p. at 10 μg per injection, 1, 3, and 5 d after cancer cell implantation.

In vivo study with NOG-SCID mice which lack functional mice effectors show that dual-xenograft of HuEC plus target cells results in greater mouse survival than single xenograft of target cells when combined with humanized anti-CD26 mAb. These data clearly corroborate the *in vitro* data, suggesting that humanized anti-CD26 mAb induces a biphasic antitumor action with a human effector system.

CD26 status may be altered in cancer and may have an effect on the growth and metastatic potential of various tumors. Absence of CD26 is associated with the development of some cancers, whereas presence of CD26 is associated with a more aggressive phenotype in other neoplasms. For example, in non-small cell lung cancer cell lines, cells transfected with CD26 develop morphologic changes, altered contact inhibition, and reduced ability for anchorage-independent growth (29). CD26 reexpression also correlates with increased $p21^{cip2/waf1}$ expression, leading to induction of apoptosis and cell cycle arrest in G_1 stage. Wesley et al. reported that CD26/dipeptidyl peptidase IV up-regulates the expression of CDKI $p27^{kip1}$ by 4-fold to 6-fold in CD26-transfected DU-145 metastatic prostate cancer cells compared with the parent and vector-transfected DU-145 cells (30). It is also reported that over-expression of CD26 in ovarian cancer leads to increased E-cadherin and tissue inhibitors of matrix metalloproteinases, resulting in decreased invasive potential (31). CD26/dipeptidyl peptidase IV thus functions as a tumor suppressor in the cases described above, and its down-regulation may contribute to the loss of growth control. In contrast, CD26 expression is associated with a more aggressive clinical course in T-cell large granular lymphocyte leukemia (32).

An earlier report indicated that CD26 and CD40L expression is mutually exclusive, with CD40L expressed on cells from more indolent diseases. Of note is that CD26 expression on T-cell LBL/ALL is associated with a worse survival (33). We now show that CD26 is highly expressed in malignant mesothelioma tissues and anti-CD26 mAb treatment and CD26 down-regulation by siRNA in CD26-positive malignant mesothelioma cell lines lead to contact inhibition and $p27^{kip1}$ up-regulation. Therefore in case of malignant tumors, such as T-cell lymphoma, and malignant mesothelioma, CD26 plays a role in tumor growth and may be involved in invasion and metastasis.

Malignant mesothelioma is an aggressive neoplasm with a dismal prognosis and is relatively unresponsive to chemotherapy. One study systematically reviewed evidence for chemotherapy effect from 1965 through June 2001 and found 83 studies with 88 treatment arms (34). Cisplatin was the most active single drug, and cisplatin with doxorubicin had the highest response rate (28.5% response rate; confidence interval, 21.3% to 35.7%). Since this report, results of a phase III randomized trial (using 448 chemotherapy naive patients with unresectable mesothelioma) involving the combination cisplatis/pemetrexed (an antimetabolite) or cisplatin alone have shown that medium survival is extended from 9.3 months in

patients treated with cisplatin to 12.1 months in patients treated with both agents (35). However, standard treatments for malignant mesothelioma are still not satisfactory in terms of survival; hence, there is an urgent need for novel therapeutic approaches for malignant mesothelioma.

Our data therefore indicate that the novel humanized anti-CD26 mAb is an effective therapeutic tool for cancer treatment including malignant mesothelioma, as it can use the human effector system to target cancer cells in addition to its direct antitumor effect.

References

1. Britton M. The epidemiology of mesothelioma. Semin Surg Oncol 2002;29:18–25.
2. Connelly RR, Spirtas R, Myers MH, Percy CL, Fraumeni JF, Jr. Demographic patterns for mesothelioma in the United States. J Natl Cancer Inst 1987;78: 1053–60.
3. Ismaril-Khan R, Robinson LA, Williams CC, Jr., Garrett CR, Bepler G, Simon GR. Malignant Pleural Mesothelioma, a comprehensive review. Cancer control 2006;13:255–63.
4. Pass H. Malignant pleural mesothelioma, surgical roles and novel therapies. Clin Lung Cancer 2001;3: 102–17.
5. Morimoto C, Schlossman SF.The structure and function of CD26 in the T-cell immune response. Immunol Rev 1998;161:55–70.
6. Ishii T, Ohnuma K, Murakami A, et al. CD26-mediated signaling for T cell activation occurs in lipid rafts through its association with CD45RO. Proc Natl Acad Sci U S A 2001;98:12138–43.
7. Ohnuma K, Yamochi T, Uchiyama M, et al. CD26 up-regulates expression of CD86 on antigen-presenting cells by means of caveolin-1. Proc Natl Acad Sci U S A 2004;101:14186–91.
8. Yamochi T, Yamochi T, Aytac U, et al. Regulation of p38 phosphorylation and topoisomerase IIα expression in the B-cell lymphoma line Jiyoye by CD26/dipeptidyl peptidase IV is associated with enhanced *in vitro* and *in vivo* sensitivity to doxorubicin. Cancer Res 2005;65:1973–83.
9. Pro B, Dang NH.CD26/dipeptidyl peptidase IV and its role in cancer. Histol Histopathol 2004;19:1345–51.
10. Iwata S, Morimoto C. CD26/dipeptidyl peptidase IV in context. The different roles of a multifunctional ectoenzyme in malignant transformation. J Exp Med 1999;190:301–6.
11. Kehlen A, Lendeckel U, Dralle H, Langner J, Hoang-Vu C. Biological significance of aminopeptidase N/CD13 in thyroid carcinomas. Cancer Res 2003;63:8500–6.
12. Kajiyama H, Kikkawa F, Suzuki T, Shibata K, Ino K, Mizutani S. Prolonged survival and decreased invasive activity attributable to dipeptidyl peptidase IV overexpression in ovarian carcinoma. Cancer Res 2002;62: 2753–7.
13. Cheng HC, Abdel-Ghany M, Pauli BU. A novel consensus motif in fibronectin mediates dipeptidyl peptidase IV adhesion and metastasis. J Biol Chem 2003; 278:24600–7.
14. Johnson RC, Zhu D, Augustin-Voss HG, Pauli BU. Lung endothelial dipeptidyl peptidase IV is an adhesion molecule for lung-metastatic rat breast and prostate carcinoma cells. J Cell Biol 1993;121:1423–32.
15. Dang NH, Torimoto Y, Schlossman SF, Morimoto C. Human CD4 helper T cell activation: functional involvement of two distinct collagen receptors. J Exp Med 1990;172:649–52.
16. Ohnuma K, Ishii T, Iwata S, et al. G_1-S cell cycle arrest provoked in human T cells by antibody to CD26. Immunology 2002;107:325–33.
17. Ho L, Aytac U, Stephens LC, et al. *In vitro* and *in vivo* antitumor effect of the anti-CD26 monoclonal antibody 1F7 on human CD30+ anaplastic large cell T-cell lymphoma Karpas 299. Clin Cancer Res 2001; 7:2031–40.
18. Inamoto T, Yamochi T, Ohnuma K, et al. Anti-CD26 monoclonal antibody-mediated G_1-S arrest of human renal clear cell carcinoma Caki-2 is associated with retinoblastoma substrate dephosphorylation, cyclin-dependent kinase 2 reduction, p27(kip1) enhancement, and disruption of binding to the extracellular matrix. Clin Cancer Res 2006;12:3470–7.
19. Usami N, Fukui T, Kondo M, et al. Establishment and characterization of four malignant pleural mesothelioma cell lines from Japanese patients. Cancer Sci 2006;97:387–94.
20. Morimoto C, Torimoto Y, Levinson G, et al. 1F7, a novel cell surface molecule, involved in helper function of CD4 cells. J Immunol 1989;143:3430–9.
21. Kobayashi S, Ohnuma K, Uchiyama M, et al. Association of CD26 with CD45RA outside lipid rafts attenuates cord blood T-cell activation. Blood 2004; 103:1002–10.
22. Tanaka J, Miwa Y, Miyoshi K, Ueno A, Inoue H. Construction of Epstein-Barr virus-based expression vector containing mini-oriP. Biochem Biophys Res Commun 1999;264:938–43.
23. Sato K, Aytac U, Yamochi T, et al. CD26/dipeptidyl peptidase IV enhances expression of topoisomerase II α and sensitivity to apoptosis induced by topoisomerase II inhibitors. Br J Cancer 2003;89:1366–74.
24. Prang N, Preithner S, Brischwein K, et al. Cellular and complement-dependent cytotoxicity of Ep-CAM-specific monoclonal antibody MT201 against breast cancer cell lines. Br J Cancer 2005;92:342–9.
25. Dang NH, Torimoto Y, Schlossman SF, Morimoto C. Human CD4 helper T cell activation: functional involvement of two distinct collagen receptors, 1F7 and VLA integrin family. J Exp Med 1990;172: 649–52.
26. Suzuki E, Nagata D, Yoshizumi M, et al. Reentry into the cell cycle of contact-inhibited vascular endothelial cells by a phosphatase inhibitor. Possible involvement of extracellular signal-regulated kinase and phosphatidylinositol 3-kinase. J Biol Chem 2000;275:3637–44.
27. Levenberg S, Yarden A, Kam Z, Geiger B. p27 is involved in N-cadherin-mediated contact inhibition of cell growth and S-phase entry. Oncogene 1999;18: 869–76.
28. Shultz LD, Schweitzer PA, Christianson SW, et al. Multiple defects in innate and adaptive immunologic function in NOD/LtSz-scid mice. J Immunol 1995; 154:180–91.
29. Wesley UV, Tiwari S, Hoghton AN. Role for dipeptidyl peptidase in tumor suppression of human non small cell lung carcinoma cells (NSCLC). Int J Cancer 2004;109:855–66.
30. Wesley UV, McGroarty M, Homoyouni A. Dipeptidyl peptidase inhibits malignant phenotype of prostate cancer cells by blocking basic fibroblast growth factor signaling pathway. Cancer Res 2005;65: 1325–34.
31. Kajiyama H, Kikkawa F, Khin E, Shibata K, Ino K, Mizutani S. Dipeptidyl peptidase overexpression induces up-regulation of E-cadherin and tissue inhibitors of matrix metalloproteinases, resulting in decreased invasive potential in ovarian carcinoma cells. Cancer Res 2003;63:2278–83.
32. Dang NH, Aytac U, Sato K, et al. T-large granular lymphocyte lymphoproliferative disorder: expression of CD26 as a marker of clinically aggressive disease and characterization of marrow inhibition. Br J Haematol 2003;121:857–65.
33. Canbon A, Gloghini A, Zagonel V, et al. The expression of CD26 and CD40 ligand is mutually exclusive in human T-cell non-Hodgkin's lymphomas/leukemias. Blood 1995;86:4617–26.
34. Berghmans T, Paesmans M, Lalami Y, et al. Activity of chemotherapy and immunotherapy on malignant mesothelioma: a systemic review of the literature with meta-analysis. Lung Cancer 2002;38:111–21.
35. Vogelzang NJ, Rusthoven JJ, Symanowski J, et al. Phase study of pemetrexed in combination with cisplatin versus cisplatin alone in patients with malignant pleural mesothelioma. J Clin Oncol 2003;21: 2629–30.

Role of Peyer's patches in the induction of *Helicobacter pylori*-induced gastritis

Shigenori Nagai*†, Hitomi Mimuro†‡, Taketo Yamada§, Yukiko Baba*†, Kazuyo Moro*, Tomonori Nochi†¶, Hiroshi Kiyono†¶, Toshihiko Suzuki†‡, Chihiro Sasakawa†‡, and Shigeo Koyasu*†‖

Departments of *Microbiology and Immunology and §Pathology, Keio University School of Medicine, Tokyo 160-8582, Japan; Divisions of ‡Bacterial Infection and ¶Mucosal Immunology, Department of Microbiology and Immunology, Institute of Medical Science, University of Tokyo, Tokyo 108-8639, Japan; and †Core Research for Evolutional Science and Technology, Japan Science and Technology Agency, Kawaguchi, Saitama 332-0012, Japan

Edited by Jeffrey I. Gordon, Washington University School of Medicine, St. Louis, MO, and approved April 12, 2007 (received for review October 12, 2006)

***Helicobacter pylori* is a Gram-negative spiral bacterium that causes gastritis and peptic ulcer and has been implicated in the pathogenesis of gastric adenocarcinoma and mucosa-associated lymphoid tissue lymphoma. Although Th1 immunity is involved in gastritis and the accumulation of *H. pylori*-specific CD4$^+$ T cells in the *H. pylori*-infected gastric mucosa in human patients, how T cells are primed with *H. pylori* antigens is unknown because no apparent lymphoid tissues are present in the stomach. We demonstrate here that Peyer's patches (PPs) in the small intestine play critical roles in *H. pylori*-induced gastritis; no gastritis is induced in *H. pylori*-infected mice lacking PPs. We also observed that the coccoid form of *H. pylori* is phagocytosed by dendritic cells in PPs. We propose that *H. pylori* converts to the coccoid form in the anaerobic small intestine and stimulates the host immune system through PPs.**

CD4 T cells | coccoid form | dendritic cells | gastric epithelial cells | inflammation

Helicobacter pylori is a Gram-negative microaerophilic bacterium that infects human gastric epithelial cell (gEC) surfaces and the overlying gastric mucin. More than 50% of the world's population is infected by *H. pylori*, although most patients have no remarkable symptoms (1). However, in some of patients, *H. pylori* infection leads to active chronic gastritis or peptic ulcer (2). In addition, *H. pylori* has also been implicated in the pathogenesis of gastric adenocarcinoma and mucosa-associated lymphoid tissue lymphoma (3). When *H. pylori* colonizes gastric mucosa, effector molecules are injected into gastric epithelial cells or the submucosal area through the type IV secretion system (1, 4). For example, the CagA effector is phosphorylated in the target cells and activates a signaling pathway to elicit growth factor-like responses. Another effector molecule, VacA, causes the massive vacuolar degradation of epithelial cells, thus disrupting the gastric epithelial barrier. VacA also interferes with the activation and proliferation of T lymphocytes within the gastric lamina propria (gLP) (5).

It was originally proposed that effector molecules, including CagA, trigger the secretion of chemokines such as IL-8 and RANTES from gECs, which attract neutrophils and mononuclear cells into the gLP (4). However, it was later shown that *H. pylori* did not induce gastritis in lymphopenic SCID mice, although gastritis was induced after adoptive transfer of naive CD4$^+$ T cells (6). The importance of CD4$^+$ T cells was underscored by the fact that *H. pylori* is not eliminated from gastric mucosa in MHC class II-deficient mice (7).

Gastritis is more severe in Th1-prone mice than Th2-prone mice on infection with the mouse-adapted *H. pylori* strain SS1 (8). Furthermore, the accumulation of *H. pylori*-specific CD4$^+$ T cells in the *H. pylori*-infected gastric mucosa in human patients (9) suggests that CD4$^+$ T cell-mediated Th1 immune responses play a critical role in *H. pylori*-induced gastritis. However, how CD4$^+$ T cells are primed by *H. pylori* antigens in the stomach where no apparent lymphoid tissues are present and how the *H. pylori*-induced chronic inflammation is maintained by T cells is unknown.

Although *H. pylori* forms an actively dividing, spiral-shaped morphology in the stomach, it is able to convert to a nonculturable, but viable, coccoid form under unfavorable conditions such as an anaerobic environment, increased oxygen tension, and long-term culture (10, 11). The coccoid form is thought to be important for transmission to new hosts by an oral–oral or oral–feces route because this form is more resistant to environmental stresses. Although the coccoid form is not culturable *in vitro*, transcription and translation actively take place in the coccoid form (12, 13). However, it is unknown whether the coccoid form is involved in the pathogenesis of *H. pylori*-induced gastritis.

In this study, we demonstrate that *H. pylori* antigen-specific CD4$^+$ T cells are necessary and sufficient for the induction of gastritis by *H. pylori*. We also demonstrate that CD4$^+$ T cells are likely primed with *H. pylori* antigens captured in the small intestine, where the coccoid form of *H. pylori* is taken up by dendritic cells (DCs) in Peyer's patches (PPs).

Results

Adoptive Transfer of Naive CD4$^+$T Cells Induces Gastritis in *H. pylori*-Infected Rag2$^{-/-}$ Mice. The *H. pylori* SS1 strain induces more severe gastritis in Th1-prone C57BL/6 than Th2-prone BALB/c mice as demonstrated by the infiltration of neutrophils and lymphocytes into the gLP and the submucosal area (Fig. 1*a* and data not shown). In contrast, when C57BL/6-Rag2$^{-/-}$ mice lacking T and B cells were infected with *H. pylori*, no gastritis was observed (Fig. 1*b*), as previously shown with SCID mice (6). The clearance of bacteria in Rag2$^{-/-}$ mice was impaired because $>10^7$ cfu/g tissues of *H. pylori* colonized the gastric mucosa (Table 1), and the colonization of *H. pylori* was readily detected by anti-*H. pylori* antibody staining (Fig. 1*c*). However, adoptive transfer of naive splenic CD4$^+$ T cells into Rag2$^{-/-}$ mice 2 months after *H. pylori* infection induced severe gastritis, with massive infiltration of neutrophils and lymphocytes into the gLP and the submucosal area (Fig. 1*d*). This massive infiltration resulted in the exclusion of colonized *H. pylori* from gastric mucosa (Table 1).

Author contributions: S.N., H.K., C.S., and S.K. designed research; S.N., H.M., T.Y., Y.B., K.M., T.N., and T.S. performed research; and S.N., C.S., and S.K. wrote the paper.

The authors declare no conflict of interest.

This article is a PNAS Direct Submission.

Abbreviations: DKO, double knockout; LP, lamina propria; gLP, gastric LP; gEC, gastric epithelial cell; DC, dendritic cell; PPs, Peyer's patches; OVA, ovalbumin; NK, natural killer; APC, antigen-presenting cell; β-Rag DKO, IL-2 receptor β chain (IL-2Rβ)$^{-/-}$Rag2$^{-/-}$ DKO; γ_c-Rag DKO, cytokine receptor common γ chain (γ_c)$^{-/-}$Rag2$^{-/-}$ DKO; GALT, gut-associated lymphoid tissue; ILF, isolated lymphoid follicle; BMDC, bone marrow-derived cell; SED, subepithelial dome; mLN, mesenteric lymph node.

‖To whom correspondence should be addressed. E-mail: koyasu@sc.itc.keio.ac.jp.

This article contains supporting information online at www.pnas.org/cgi/content/full/0609014104/DC1.

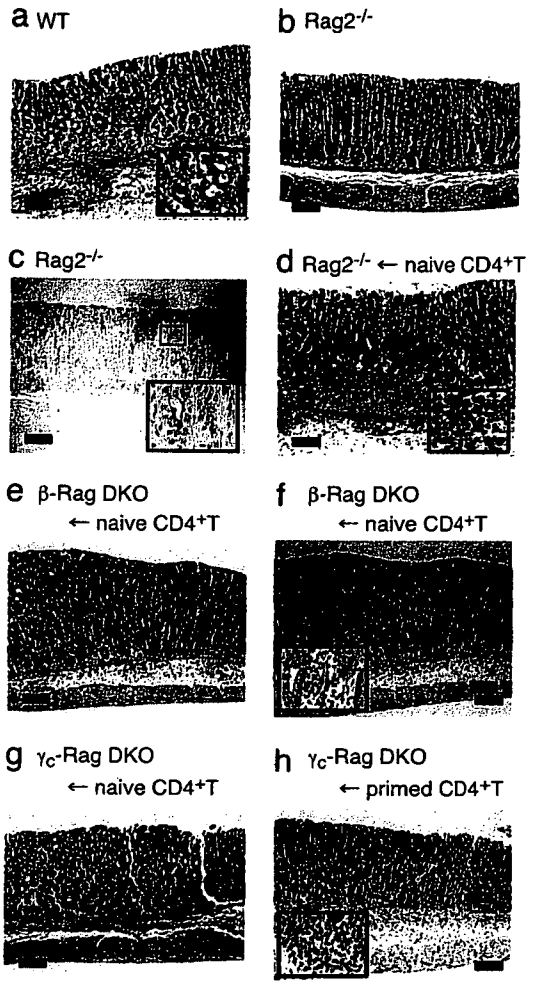

Fig. 1. Naive CD4+ T cells did not induce gastritis in *H. pylori*-infected γ_c-Rag double knockout (DKO) mice. (*a–c*) Wild-type (*a*) or Rag2$^{-/-}$ (*b* and *c*) mice were infected with *H. pylori*. Two months after the infection, gastric specimens were prepared. (*d–h*) Rag2$^{-/-}$ (*d*), β-Rag DKO (e and *f*), and γ_c-Rag DKO (*g* and *h*) mice were infected with *H. pylori*. Two months after the infection, naive (*d–g*) or primed (*h*) splenic CD4+ T cells were transferred. Two months after the cell transfer, gastric specimens were stained with H&E (*a*, *b*, *d*, e, *g*, and *h*), anti-*H. pylori* antisera (brown) (*c*), or chloroacetate esterase (red) for infiltrated neutrophils and mast cells (*f*). (Scale bars: 200 μm.)

***H. pylori* Antigen-Specific CD4+ T Cells Are Indispensable for Induction of Gastritis.** Primary gECs secrete MIP-2, a functional homolog of IL-8, on *H. pylori* infection *in vitro*, and the amount produced by Rag2$^{-/-}$ gECs was comparable to that produced by wild-type gECs [supporting information (SI) Fig. 5*a*]. CD4+ T cells isolated from the gLP of *H. pylori*-infected mice were able to produce larger amounts of MIP-2 than splenic CD4+ T cells from the same mice in response to *H. pylori* antigens (SI Fig. 5*b*). Moreover, the amounts of MIP-2 produced by gLP CD4+ T cells were much larger than those produced by gECs (compare SI Fig. 5 *a* and *b*). The importance of CD4+ T cells for neutrophil infiltration on *H. pylori* infection was further confirmed by the depletion of CD4+ T cells from wild-type mice that had already developed gastritis by *H. pylori* infection. After depleting CD4+ T cells by the i.v. injection of anti-CD4 mAb, the gastritis became milder (Table 1 and SI Fig. 6 *a* and *b*), and the number of bacteria in the gastric mucosa increased (Table 1). These results indicate the critical role of CD4+ T cells for both triggering and maintaining gastritis. When CD4+ T cells from OT-II transgenic mice on a Rag2$^{-/-}$ background (OT-II-Rag mice), specific for an ovalbumin ($OVA_{323-339}$ peptide on an MHC class II molecule I-A^b), were transferred into *H. pylori*-infected Rag2$^{-/-}$ mice, no gastritis was induced (SI Fig. 6*c*). Similarly, when OT-II-Rag mice were infected with *H. pylori*, no gastritis was induced despite the presence of CD4+ T cells (Table 1 and SI Fig. 6*d*). Furthermore, when OVA protein or $OVA_{323-339}$ peptide was administered into *H. pylori*-infected OT-II-Rag mice, no inflammation was observed, although CD4+ T cells were activated in these mice (Table 1, SI Fig. 6*e*, and data not shown). These results collectively indicate the importance of *H. pylori* antigen recognition by CD4+ T cells in the induction of gastritis.

CD4+ T Cells Are Not Primed with *H. pylori* Antigen in γ_c-Rag DKO Mice. IFNγ, a key cytokine for Th1 immune responses, is important for the pathogenesis of *H. pylori*-induced gastritis (14). Natural killer (NK) cells and antigen-presenting cells (APCs) including DCs are able to produce IFNγ to prevent bacterial infection (15). The interaction between DCs and NK cells enhances the production of IFNγ during *H. pylori* infection (16, 17). To test the importance of DC–NK interaction in the *H. pylori*-induced inflammatory response, we transferred splenic CD4+ T cells into *H. pylori*-infected IL-2 receptor β chain (IL-2Rβ)$^{-/-}$Rag2$^{-/-}$ (β-Rag DKO) mice and cytokine receptor common γ chain (γ_c)$^{-/-}$Rag2$^{-/-}$ DKO (γ_c-Rag DKO) mice. These mice lack NK cells because of impaired IL-15 signaling, which is critical for NK cell development (18, 19). In addition, the production of IL-12 and IFNγ by APCs from these mice is impaired (20). As shown in Fig. 1 *e* and *f*, gastritis was induced in *H. pylori*-infected β-Rag DKO mice when naive CD4+ T cells were transferred. Clearance of bacteria was also achieved by the naive CD4+ T cell transfer (Table 1), indicating that NK cells and NK–DC interaction are dispensable for the induction of gastritis by *H. pylori* infection.

Surprisingly, there was no gastritis induced in γ_c-Rag DKO mice even after the transfer of naive CD4+ T cells (Fig. 1*g*), NK cells (SI Fig. 7*a*), or NK cells with naive CD4+T cells (SI Fig. 7*b*), suggesting that γ_c-Rag DKO mice have additional defects compared with β-Rag DKO mice. Interestingly, when splenic CD4+ T cells isolated from *H. pylori*-infected wild-type mice were transferred, gastritis was induced in *H. pylori*-infected γ_c-Rag DKO mice (Fig. 1*h*), and the clearance of bacteria was evident (Table 1). These results suggest that CD4+ T cells were not primed in γ_c-Rag DKO mice. In fact, splenocytes from these mice did not respond to DCs preincubated with *H. pylori* lysate, whereas splenocytes from wild-type mice infected with *H. pylori* strongly responded and produced IFNγ in response to the same DC preparation (data not shown). It should be noted that there were no apparent defects in DCs from γ_c-Rag DKO mice compared with those from wild-type mice with regard to their ability to induce T cell activation and present antigen as examined by the induction of CD69 expression and IFNγ production by splenic CD4+ T cells (SI Fig. 8).

PPs Are a Critical Tissue for Priming CD4+T Cells with *H. pylori* Antigen. One difference between β-Rag DKO and γ_c-Rag DKO mice is that the latter lack gut-associated lymphoid tissues (GALT) such as PPs and isolated lymphoid follicles (ILFs) due to impaired IL-7 signaling (21) (Fig. 2 *a–d*). Thus, we hypothesized that CD4+ T cells are primed in GALT such as PPs or ILFs. To test this possibility, we generated PP-null mice by administration of anti-IL-7Rα mAb *in utero* (22) (Fig. 2 *e* and *f*). As observed in γ_c-Rag DKO mice, no gastritis was induced in PP-null mice 2 months after *H. pylori* infection, and a large number of *H. pylori* was detected in the gastric mucosa (Fig. 2 *h* and *i* and Table 1). We also generated PP-null mice on a Rag2$^{-/-}$ background (PP-null-Rag2$^{-/-}$ mice) (Fig. 2*g*). The adoptive transfer of CD4+ T cells from *H. pylori*-infected wild-type mice, but not naive CD4+ T cells, induced strong inflammation in PP-null-Rag2$^{-/-}$

Table 1. PP-dependent bacterial clearance in *H. pylori* infection

Mouse*	*n*	Cells transferred†	Bacterial colonization,‡ cfu/g tissue × 10^{-6}	Neutrophils, average (range)	Active inflammation, average (range)	GAIS,§ average (range)
Wild type	7	None	2.2 ± 1.3	1.6 (0–3)	1.4 (0–3)	13.6 (0–34)
Wild type	4	$CD4^+$ T cell-depleted	25 ± 7	0 (0)	1.0 (0–2)	0 (0)
$Rag2^{-/-}$	4	None	14 ± 4	0 (0)	0 (0)	0 (0)
$Rag2^{-/-}$	5	Naive $CD4^+$ T	0.15 ± 0.17	2.0 (2)	2.0 (2)	5.0 (2–8)
$Rag2^{-/-}$	5	OT-II-Rag $CD4^+$ T	34 ± 11	0 (0)	0 (0)	0 (0)
β-Rag DKO	4	Naive $CD4^+$ T	0.67 ± 0.39	1.5 (1–2)	1.3 (1–2)	9.2 (3–18)
γ_c-Rag DKO	6	Naive $CD4^+$ T	18 ± 11	0 (0)	0 (0)	0 (0)
γ_c-Rag DKO	6	Primed $CD4^+$ T	0.22 ± 0.39	0.66 (0–1)	1.5 (0–2)	1.6 (0–5)
γ_c-Rag DKO	3	Primed $CD4^+$ T from PPs	<0.01	1.0 (1)	2.0 (2)	1.0 (0–2)
γ_c-Rag DKO	3	Primed $CD4^+$ T from mLN	0.88 ± 0.78	0.5 (0–1)	1.5 (1–2)	4.0 (3–5)
γ_c-Rag DKO	3	Primed $CD4^+$ T by coccoid form	1.8 ± 1.6	0.33 (0–1)	0.66 (0–1)	2.0 (0–6)
PP-null-wild type	8	None	16 ± 9	0 (0)	0.37 (0–1)	0 (0)
PP-null-$Rag2^{-/-}$	3	Naive $CD4^+$ T	5.3 ± 4.0	1.0 (0–2)	1.0 (0–2)	4 (0–7)
PP-null-$Rag2^{-/-}$	3	Primed $CD4^+$ T	0.53 ± 0.28	2.6 (2–3)	2.6 (2–3)	21 (13–33)

*All mice were on a C57BL/6 background. Although not shown, the degrees of bacterial colonization in β-Rag DKO, γ_c-Rag DKO, and PP-null-$Rag2^{-/-}$ mice without $CD4^+$ T cell transfer were similar to those of $Rag2^{-/-}$ mice.

†Splenocytes were used for cell transfer unless otherwise stated. Five million cells were transferred except for the transfer of PP-derived cells, where 5×10^5 cells were used.

‡Mean ± SD.

§Gland active inflammatory score. See *Materials and Methods*.

mice just as in the γ_c-Rag DKO mice (Fig. 2 *j* and *k* and Table 1). These results strongly suggest that PPs are critical for priming $CD4^+$ T cells in *H. pylori* infection, but dispensable for the effector phase.

The Coccoid, but Not Helical, Form of *H. pylori* Is Phagocytosed by DCs in PP. Although *H. pylori* is helical in the stomach, it transforms to the coccoid form under anaerobic conditions, such as in the small intestine (23). Interestingly, the coccoid form of *H. pylori* induced higher IL-12 production from bone marrow-derived cells (BMDCs) than the helical form (SI Fig. 9). There is a possibility that *H. pylori* transforms to the coccoid form in the intestine and is then captured by DCs present in PPs to induce a Th1 response. To test this possibility, the coccoid and helical forms of *H. pylori* were inoculated into ligated small intestinal loops. As shown in Fig. 3*a*, immunofluorescence staining detected *H. pylori* in the subepithelial dome (SED) region of PPs in a time-dependent manner, and the number of bacteria in the SED region inoculated with the coccoid form was larger than that inoculated with the helical form of *H. pylori*. In addition, double immunofluorescence staining with anti-*H. pylori* antibody and anti-CD11c mAb demonstrated that the bacteria were captured by $CD11c^+$ DCs in the SED region (Fig. 3*b*). Although the helical form of *H. pylori* kept the rod shape 1.5 h after inoculation (SI Fig. 10 *a* and *b*), the bacteria phagocytosed by $CD11c^+$ DCs in PPs were round (SI Fig. 10 *c* and *d*). These results suggest that the coccoid, but not the helical, form of *H. pylori* is captured by DCs in PPs and activates immune responses by generating *H. pylori*-specific pathogenic $CD4^+$ T cells. Consistent with this observation, $CD4^+$ T cells from the PPs as well as mesenteric lymph node (mLN) of *H. pylori*-infected wild-type mice were also able to eliminate the bacteria in γ_c-Rag DKO mice infected with *H. pylori* (Table 1).

When wild-type mice were infected with the coccoid form of *H. pylori*, gastritis was not induced because the coccoid form of *H. pylori* was unable to colonize in the stomach (Fig. 4*a* and data not shown). However, $CD4^+$ T cells from these mice induced gastritis in γ_c-Rag DKO mice infected with the helical form of *H. pylori* (Fig. 4 *b* and *c* and Table 1). These results indicate that $CD4^+$ T cells primed with the coccoid form of *H. pylori* in the intestine are sufficient to induce inflammation in the stomach infected with the helical form of *H. pylori*.

Discussion

We showed here that *H. pylori* antigen-specific $CD4^+$ T cells are required to induce and maintain gastritis on infection with *H. pylori*. Because *H. pylori* interacts with and injects pathological molecules into gECs, it is generally thought that neutrophils infiltrating the gLP are attracted by chemokines produced by gECs. However, neutrophil infiltration was not observed in $Rag2^{-/-}$ mice, although gECs of $Rag2^{-/-}$ mice were able to secret MIP-2 on *H. pylori* infection. Thus, the secretion of chemokines by gECs seems insufficient for the induction of gastritis. In addition, adoptive transfer of $CD4^+$ T cells recognizing *H. pylori*-independent antigens did not induce gastritis, suggesting that *H. pylori*-specific $CD4^+$ T cells directly or indirectly regulate production of chemokines that attract neutrophils. In fact, a large amount of MIP-2 was produced by activated $CD4^+$ T cells derived from the gLP of *H. pylori*-infected mice. In addition, infiltrated neutrophils were located around $CD4^+$ T cells in the gLP of *H. pylori*-infected mice (data not shown). It is known that another keratinocyte-derived chemokine is able to recruit neutrophils. However, the amounts of keratinocyte-derived chemokine produced by both gECs and CD4 T cells were much lower than those of MIP-2 (data not shown).

Oral or intra-PP immunization with *H. pylori* antigens was effective in enhancing *H. pylori*-specific $CD4^+$ T cell responses and reducing *H. pylori* colonization in the stomach (24, 25). These reports are consistent with our current observation that PPs play critical roles in priming $CD4^+$ T cells, and *H. pylori* is indeed captured by DCs in PPs. *H. pylori* antigen-specific $CD4^+$ T cells would be primed by DCs in PPs or mLNs where DCs migrate after capturing antigens. Interestingly, $CD4^+$ T cells cannot be primed by DCs in the gLP or gEC, both of which are capable of expressing class II MHC and presenting antigens. The lack of antigen presentation is partly due to the fact that the helical form of *H. pylori* is resistant to phagocytosis in a type IV secretion system-dependent manner, although the molecular mechanisms of antiphagocytic activity remain to be determined (26). It should be noted that the transformation of the helical to the coccoid form is accompanied by changes in the composition

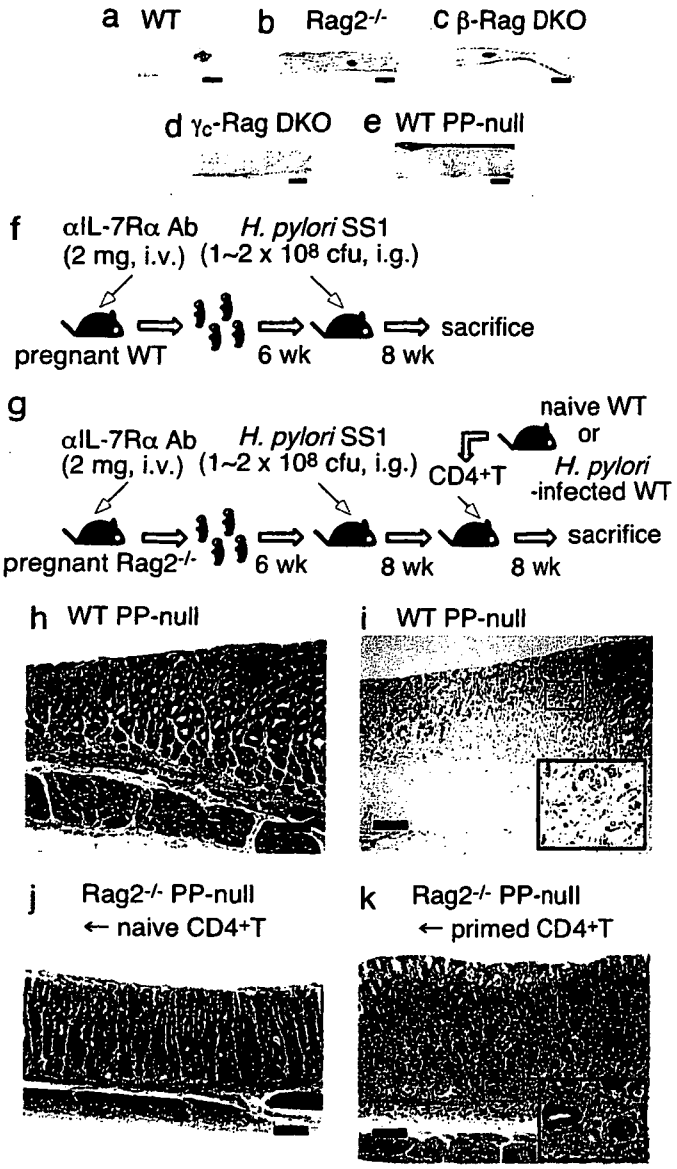

Fig. 2. PPs are critical for the priming of CD4+ T cells in *H. pylori* infection. (*a–e*) Small intestines from wild-type (WT) (*a*) and PP-null (*e*) mice were stained with anti-B220 mAb, and small intestines from Rag2$^{-/-}$ (*b*), β-Rag DKO (*c*), and γ_c-Rag DKO (*d*) mice were stained with anti-CD45 mAb. (*f* and *g*) Schemes of the generation of PP-null WT (*f*) or PP-null-Rag2$^{-/-}$ (*g*) mice. (*h* and *i*) PP-null WT mice were infected with *H. pylori*. Two months after the infection, gastric specimens were prepared. (*j* and *k*) PP-null-Rag2$^{-/-}$ mice were infected with *H. pylori*. Two months after the infection, naive (*j*) or primed (*k*) splenic CD4+ T cells were transferred. Two months after the cell transfer, gastric specimens were prepared. Specimens were stained with H&E (*h*, *j*, and *k*) or anti-*H. pylori* antisera (brown) (*i*). (Scale bars: 200 μm.)

of surface proteins and/or carbohydrates, which may make the bacteria susceptible to phagocytosis (27, 28), a subject worthy of further studies. It has been shown that mast cells are able to present *H. pylori* antigens to *H. pylori*-specific CD4+ T cells, which in turn activate mast cells to degranulate (29). When we infected W/W^v and Sl/Sl^d mice lacking mast cells with *H. pylori*, gastritis was readily induced in both strains of mice on infection (S.N., T.Y., Y.B., and S.K., unpublished data), indicating that mast cells are not essential in priming CD4+ T cells. In an *in vitro* experiment, BMDCs infected with the coccoid form of *H. pylori* produced larger amounts of IL-12 than those infected with the helical form of *H. pylori*, suggesting that the coccoid form of

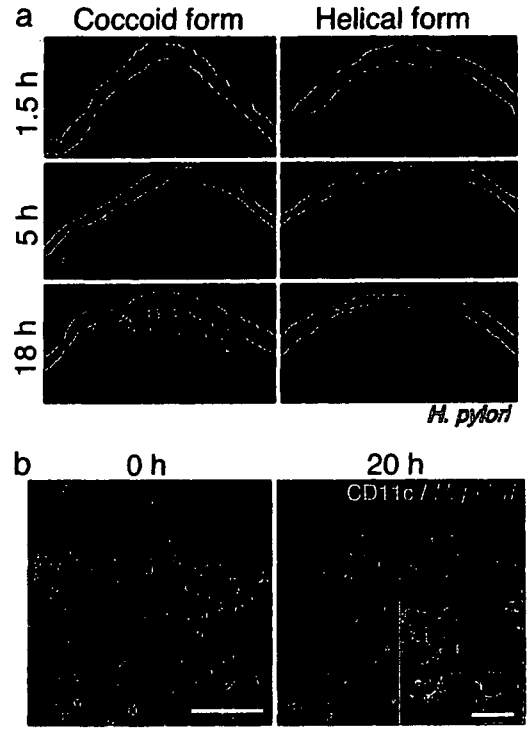

Fig. 3. The coccoid form of *H. pylori* is captured by DCs in PPs. The coccoid or helical form of *H. pylori* was inoculated into the ligated small intestines of wild-type mice. (*a*) After the indicated incubation times, PPs were stained with anti-*H. pylori* antibody. (*b*) Twenty hours after inoculation of the coccoid form, PPs were stained with anti-CD11c mAb (green) and anti-*H. pylori* antibody (red). (Scale bars: 0 h,100 μm; 20 h, 20 μm.)

H. pylori easily induces Th1 immune responses on *H. pylori* infection.

Importantly, CD4+ T cells primed with the coccoid form of *H. pylori* were able to induce gastritis in *H. pylori*-infected GALT-null γ_c-Rag DKO mice where CD4+ T cells are not

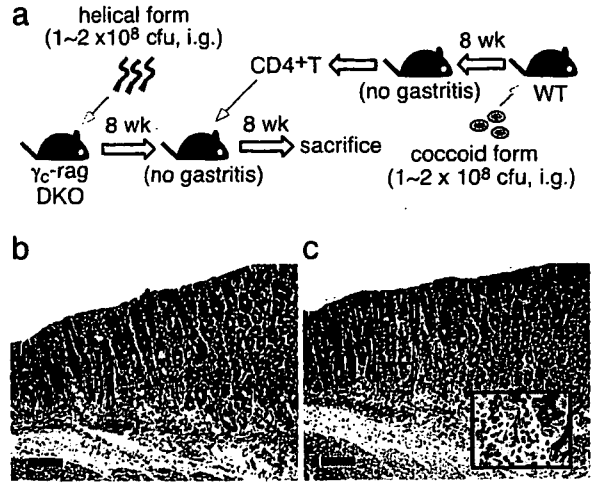

Fig. 4. Gastritis is induced by CD4+ T cells primed by the coccoid form of *H. pylori*. Two months after infection of γ_c-Rag DKO mice with the helical form of *H. pylori*, splenic CD4+ T cells from wild-type (WT) mice orally infected by the coccoid form of *H. pylori* were transferred to the infected γ_c-Rag DKO mice (*a*). Two months after the cell transfer, gastric specimens were prepared. Specimens were stained with H&E (*b*) or chloroacetate esterase (red) for infiltrated neutrophils and mast cells (*c*). (Scale bars: 200 μm.)